PLEASE CITE THIS ARTICLE AS DOI: 10.1116/6.0002722

Effect of Drift Layer Doping and NiO Parameters in Achieving 8.9 kV Breakdown in 100 μm Diameter and 4kV /4A in 1mm Diameter NiO/β-Ga₂O₃ Rectifiers

Running title: 8.9 kV Breakdown in NiO/β-Ga₂O₃ Rectifiers

Running Authors: Li et al.

Jian-Sian Li¹, Chao-Ching Chiang¹, Xinyi Xia¹, Hsiao-Hsuan Wan¹, Fan Ren¹ and S.J. Pearton ^{2,a)}

¹Department of Chemical Engineering, University of Florida, Gainesville, FL 32606 USA ²Department of Materials Science and Engineering, University of Florida, Gainesville, FL 32606 USA

a) Electronic mail: spear@mse.ufl.edu

The effect of doping in the drift layer and the thickness and extent of extension beyond the cathode contact of a NiO bilayer in vertical NiO/β-Ga₂O₃ rectifiers is reported. Decreasing the drift layer doping from $8x10^{15}$ to $6.7x10^{15}$ cm⁻³ produced an increase in reverse breakdown voltage (V_B) from 7.7kV to 8.9 kV, the highest reported to date for small diameter devices (100µm). Increasing the bottom NiO layer from 10 to 20 nm did not affect the forward current-voltage characteristics but did reduce reverse leakage current for wider guard rings and reduced the reverse recovery switching time. The NiO extension beyond the cathode metal to form guard rings had only a slight effect (~5%) in reverse breakdown voltage. The use of NiO to form a pn heterojunction made a huge improvement in V_B compared to conventional Schottky rectifiers, where the breakdown voltage was ~1kV. The on-state resistance (Ro_N) was increased from 7.1 mΩ.cm² in Schottky rectifiers fabricated on the same wafer to 7.9 m Ω .cm² in heterojunctions. The maximum power figure of merit (V_B)²/R_{ON} was 10.2 GW.cm⁻² for the 100µm NiO/Ga₂O₃ devices. We also fabricated large area (1 mm²) devices on the same wafer, achieving V_B of 4 kV and 4.1 A forward current. The figure-of-merit was 9 GW.cm⁻² for these devices. These parameters are the highest reported for large area Ga₂O₃ rectifiers. Both the small

PLEASE CITE THIS ARTICLE AS DOI: 10.1116/6.0002722

area and large area devices have performance exceeding the unipolar power device performance of both SiC and GaN.

I. INTRODUCTION

The increasing electrification of automobiles and the need to switch renewable energy sources in the existing power grid has increased demand for energy efficient power electronica capable of higher voltage and currents than existing Si devices. This has focused attention on the wide and ultra-wide bandgap semiconductors (1-5), with the latter including diamond, AlN and Ga₂O₃. The ability to grow large diameter, high quality crystals from melt-grown methods and the attendant low cost of production has spurred interest in β -Ga₂O₃ (1-5). One of the goals is to achieve a high -power figure of merit for power electronic devices, defined as $(V_B)^2/R_{ON}$ where V_B is the reverse breakdown voltage and R_{ON}- is the on-state resistance ^(1,3,4). To achieve a high-power figure of merit, a rectifier must have a low drift layer concentration, with high electron mobility, as well as low Ron, and optimized edge termination to prevent current crowding (1,5-21)). The breakdown voltage is larger for thicker drift layers, but this degrades onresistance. To achieve a low Ron, a thin drift layer with high electron mobility is required. In addition, vertical geometry devices are desirable, because of their higher power conversion efficiency and absolute currents compared to lateral devices (1,3,4,5). Power rectifiers are also building blocks for many advanced power handling systems.

A drawback with Ga₂O₃ is the absence of facile p-type doping. All of the potential acceptor dopants have large ionization energies and are not significantly ionized at room temperature. This has led to the use of p-type oxides, principally polycrystalline NiO, to form p-n heterojunctions with n-type Ga₂O₃ (6-14). The forward current transport mechanism in such junctions is typically recombination at low biases and trap-assisted

PLEASE CITE THIS ARTICLE AS DOI: 10.1116/6.0002722

tunneling at higher bias ^(10, 21-26). Promising rectifier performance has been reported with this approach ^(12-14, 21-39), including V_B of 8.32 kV, with figure of merit 13.2 GW.cm^{-2 (12)}.

Optimization of the heterojunction rectifier device structure is crucial to achieve both high V_B and low R_{ON}, as well as providing management of the maximum electric fields within the structure to enhance further the device voltage blocking capability ⁽⁴¹⁻⁴⁷⁾. The design variables include the thickness and doping of the layers, doping in the drift layer and the use of the NiO as a guard ring by extending it beyond the metal cathode. In this paper we report an investigation of the effect of these parameters on the performance of NiO/Ga₂O₃ vertical rectifiers. A new highest V_B for these devices is achieved.

II. EXPERIMENTAL

We made both vertical geometry Schottky rectifiers and NiO/ Ga_2O_3 rectifiers on the same wafers. The parameters investigated are shown in the schematic of the vertical heterojunction rectifiers in Figure 1. We varied the thickness of the second layer in the bilayer NiO (10 or 20 nm, with fixed thickness of the top layer held constant at 10 nm) and the length of the NiO extension beyond the cathode contact (12-20 μ m) to form guard rings. The choice of these parameters was guided by TCAD simulations with the Silvaco Atlas code of electric field distributions, as reported previously (14). Finally, we had two different drift region doping levels at a fixed thickness of 10 μ m. The epitaxial layers were grown by halide vapor phase epitaxy (HVPE) on a (001) Sn-doped (10¹⁹ cm⁻³) β -Ga₂O₃ single crystal substrate. These samples were purchased from Novel Crystal Technology, Japan.

PLEASE CITE THIS ARTICLE AS DOI: 10.1116/6.0002722

Ohmic contacts were made to the rear surface using a Ti/Au metal stack deposited by e-beam evaporation. This was annealed at 550°C for 180s under N₂. The front surface was exposed to UV/Ozone exposure for 15 mins to remove contamination. The NiO bilayer was deposited by rf (13.56 MHz) magnetron sputtering at a working pressure of 3mTorr ^(14,41). The hole concentration in these films was adjusted using the Ar/O₂ ratio. The structure was then annealed at 300°C under O₂. Finally, a cathode contact of 20/80 nm Ni/Au (100 µm diameter) was deposited onto the NiO layer. The NiO was extended from 12-20 um beyond the contact metal to form a guard ring. Figure 2 shows the C⁻²-V plots for the two different drift layer doping levels. These show the carrier concentrations were 6.7x10¹⁵ cm⁻³ and 8x10¹⁵ cm⁻³, respectively.

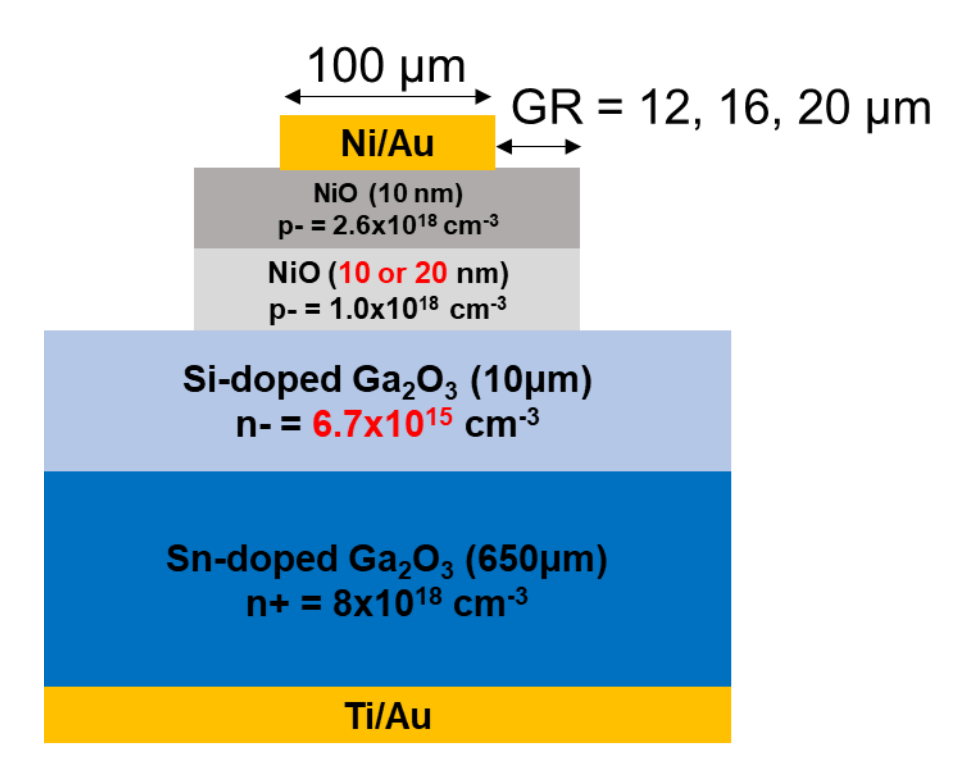


Fig 1. Schematic of NiO/Ga₂O₃ heterojunction rectifier. The extension of the NiO beyond the Ni/Au contact to act as a guard ring was investigated for different extension lengths, as well as the thickness of the bottom NiO layer and the drift layer doping.

PLEASE CITE THIS ARTICLE AS DOI: 10.1116/6.0002722

The current density-voltage (J-V) characteristics were measured on a Tektronix 370-A curve tracer, 371-B curve and Agilent 4156C. For the highest reverse voltages, a Glassman power supply was employed. The reverse breakdown voltage was defined as the bias for a reverse current reaching 0.1 A.cm². The high bias measurements were performed in Fluorinert atmosphere at 25°C. The devices did not suffer permanent damage at this condition but increasing the voltage a further 50-200 V led to permanent failure through breakdown at the contact periphery. The on-resistance values were calculated assuming the current spreading length is 10 um and a 45° spreading angle. We also subtracted the resistance of the cable, probe and chuck, which was around 10 Ohm.

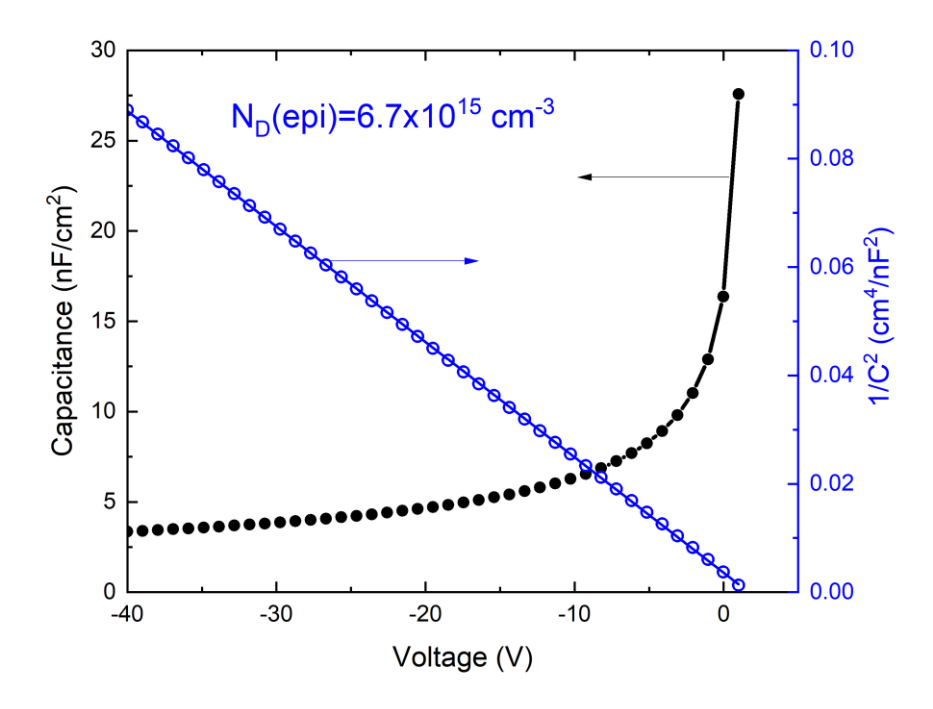


Fig. 2. C-V characteristics for determining carrier density in drift region for the two different types of wafers investigated. The drift layer thickness was $\sim 10 \,\mu m$ in both cases.

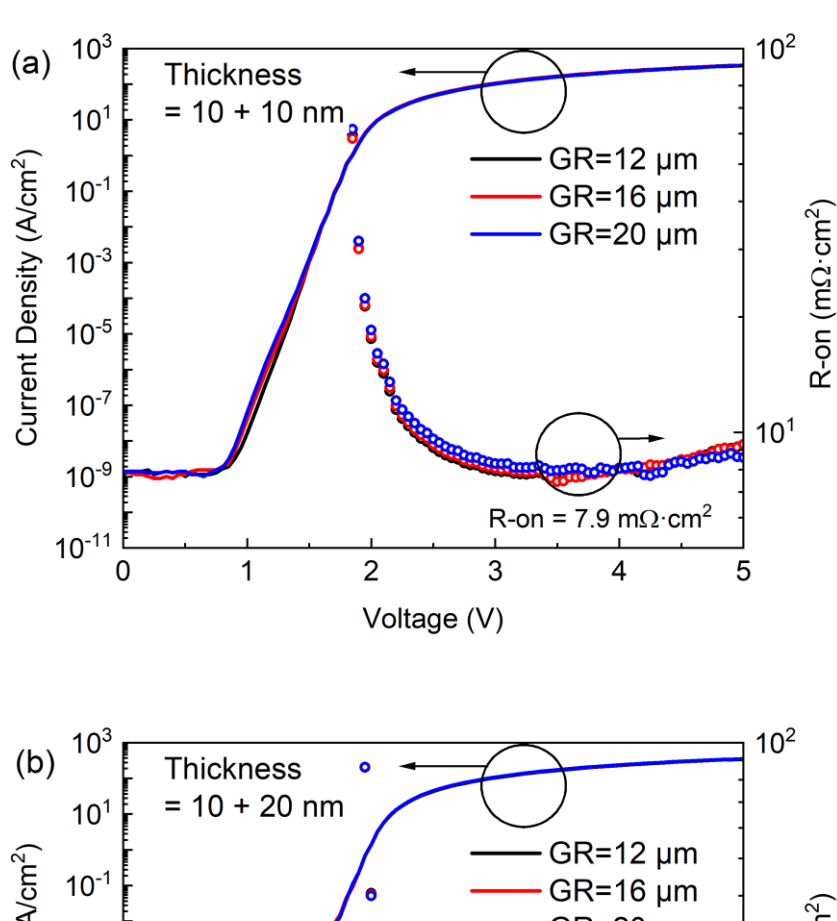
III. RESULTS AND DISCUSSION

PLEASE CITE THIS ARTICLE AS DOI: 10.1116/6.0002722

A. Small Area Rectifiers to Achieve High Breakdown Voltage

Figure 3 shows the forward current densities and R_{ON} values for rectifiers with different guard ring dimensions fabricated with (a) 10/10 nm NiO bilayer or (b) 10/20 nm NiO bilayer. These were fabricated on the drift region with the lower carrier density. There is very little difference in these forward current density characteristics for either the NO bilayer thickness or the guard ring diameter.

PLEASE CITE THIS ARTICLE AS DOI: 10.1116/6.0002722



Current Density (A/cm²) R-on ($m\Omega \cdot cm^2$) GR=20 µm 10^{-3} 10⁻⁵ 10⁻⁷ 10¹ 10⁻⁹ R-on = 7.9 m Ω ·cm² 10⁻¹¹ 2 1 3 5 4 Voltage (V)

Fig. 3. Forward current densities and Ron values for rectifiers with different guard rings dimensions fabricated with (a) 10/10 nm NiO bilayer or (b) 10/20 nm NiO bilayer.

Figure 4 shows a comparison of the results from the NiO/Ga₂O₃ heterojunction rectifiers with the Schottky rectifier fabricated on the same wafer. The on-resistance for

PLEASE CITE THIS ARTICLE AS DOI: 10.1116/6.0002722

the former was 7.9 m Ω . cm⁻². For the Schottky rectifiers, this parameter was slightly lower, as expected, at 7.1 m Ω .cm². Both types of devices had forward current densities > 100 A.cm⁻² at 5 V. The turn-on voltage was 1.9-2.1 V for the heterojunction rectifiers.

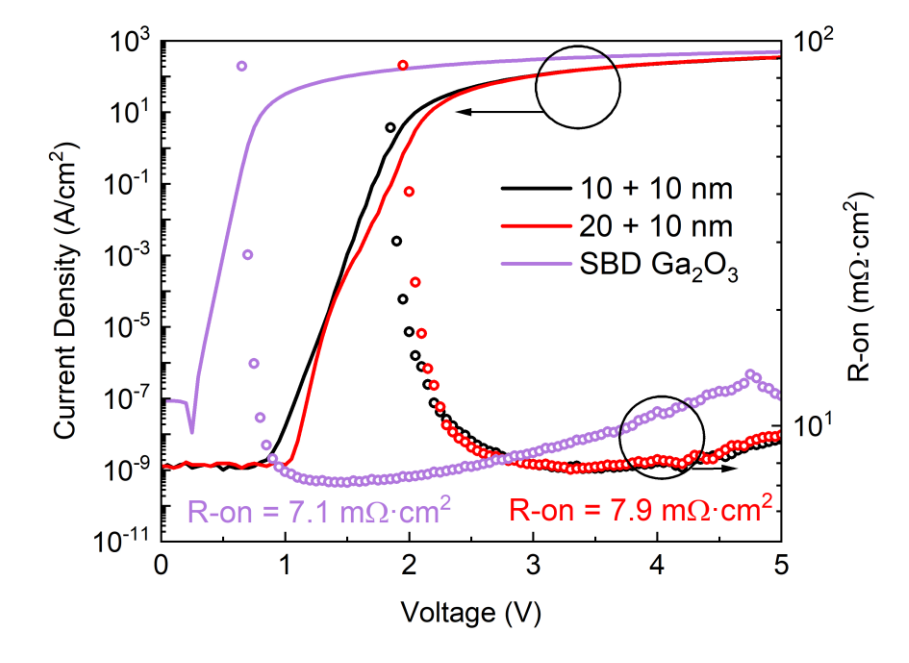
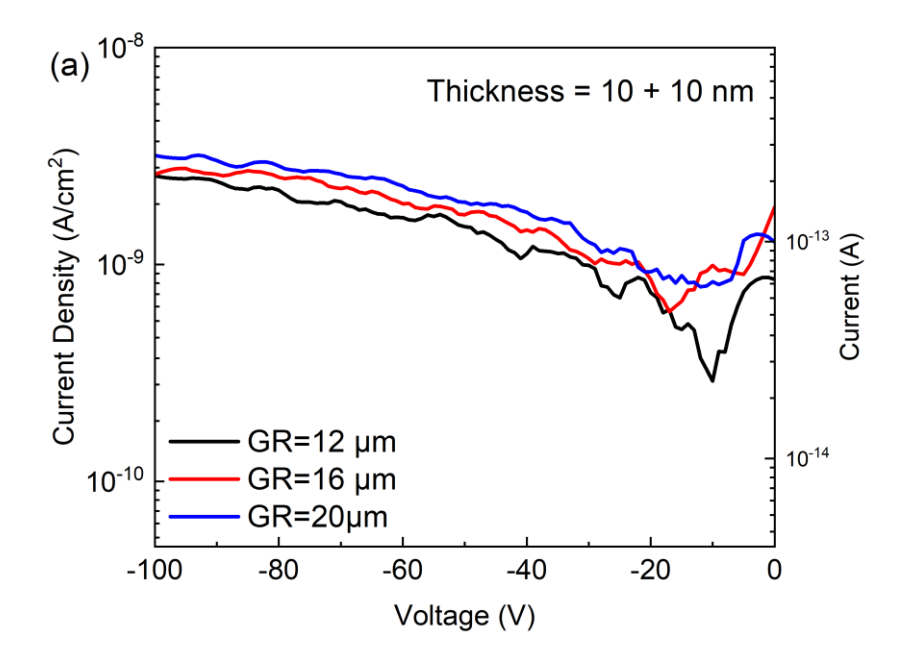


Fig. 4 Comparison of forward current density characteristics for Schottky and NiO/Ga₂O₃ rectifiers.

Figure 5 shows the reverse I-V characteristics out to -100V for (a) NiO/Ga₂O₃ rectifiers with 10/10 nm NiO bilayers or (b) 10/20 nm NiO bilayers. While the guard ring diameter makes little difference to devices with the 10/10 nm NiO bilayer, there is a reduction in reverse current density for the smaller guard rings. A comparison of the heterojunction results with those from the Schottky rectifiers all fabricated on the lower drift layer doping structure is shown in Figure 6 for a fixed guard ring diameter of 12 μm in the latter type of device. As expected, the leakage current from the heterojunction rectifiers is lower than that of the Schottky rectifier and reducing the doping in the drift layer also lowers the reverse current density (20,21,48-51). Similar trends were observed for

PLEASE CITE THIS ARTICLE AS DOI: 10.1116/6.0002722

the two types of devices fabricated on the higher drift layer doping. The p-n junction has a larger effective barrier for current transport than the metal gate Schottky rectifiers.



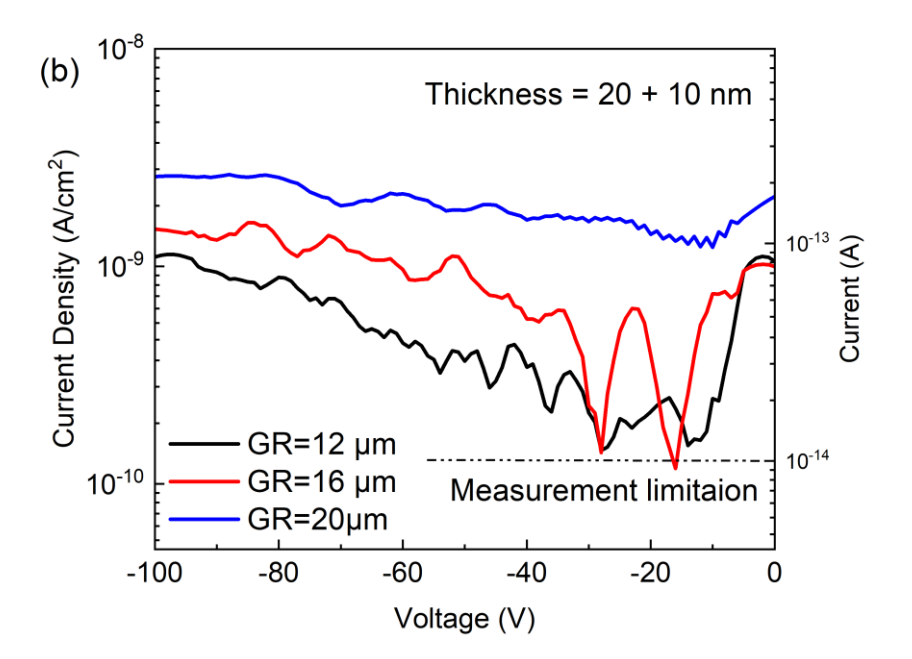


Fig. 5. Reverse I-V characteristics out to -100V for (a) NiO/Ga₂O₃ rectifiers with 10/10 nm NiO bilayers or (b) 10/20 nm NiO bilayers.

PLEASE CITE THIS ARTICLE AS DOI: 10.1116/6.0002722

10⁻¹¹ 10⁻⁷ Current Density (A/cm²) 10⁻⁸ 10⁻⁹ 10⁻¹⁴ 10 + 10 nm 20 + 10 nm SBD Ga₂O₃ 10⁻¹⁵ 10⁻¹¹ -80 -60 -40 -20 -100 0 Voltage (V)

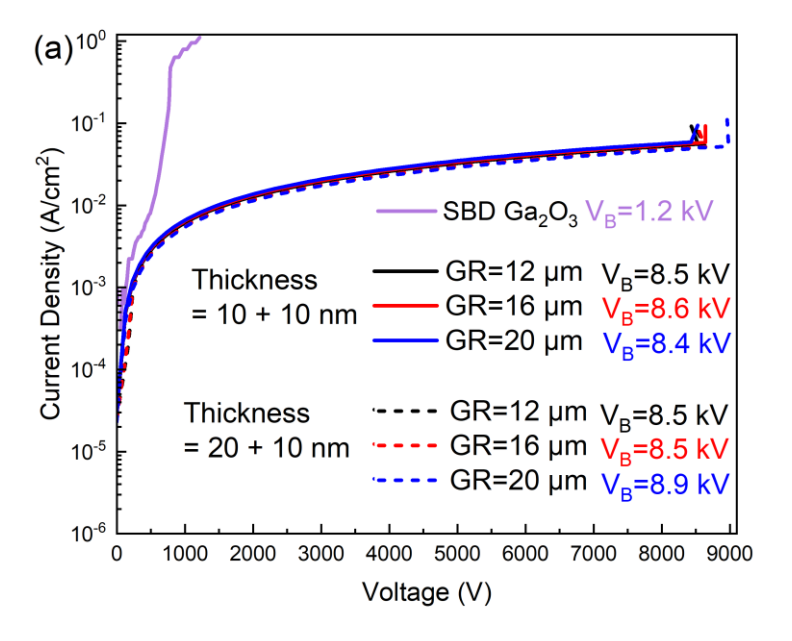
10⁻⁶

Fig. 6. Comparison of low bias reverse current characteristics between Schottky rectifiers and NiO/Ga₂O₃ rectifiers with either 10/10 nm or 10/20 nm bilayers. All these were fabricated on the sample with drift layer doping 6.7×10^{15} cm⁻³.

The reverse J-V characteristics over the full bias range are shown in Figure 7 (a) for the devices fabricated on the 6.7 x10¹⁵ cm⁻³ drift layers with different NiO thicknesses as well as different guard ring diameters. Once again, for comparison, we show the result for the Schottky rectifier and for a heterojunction device fabricated ion the wafer with larger drift layer concentration of 8x10¹⁵ cm⁻³. The key points from this data are firstly, that the lower doping produces a higher reverse breakdown voltage, with a maximum of 8.9 kV. This is the highest reported to data for Ga₂O₃ rectifiers of any type (12). The second point is that the heterojunction really increases reverse breakdown voltage compared to the Schottky rectifier. The V_b of the latter was 750V, while the

PLEASE CITE THIS ARTICLE AS DOI: 10.1116/6.0002722

device reached 1218 V before permanent burn out. The final point is that the NiO thickness and guard ring extension length made only a relatively small difference in V_B.



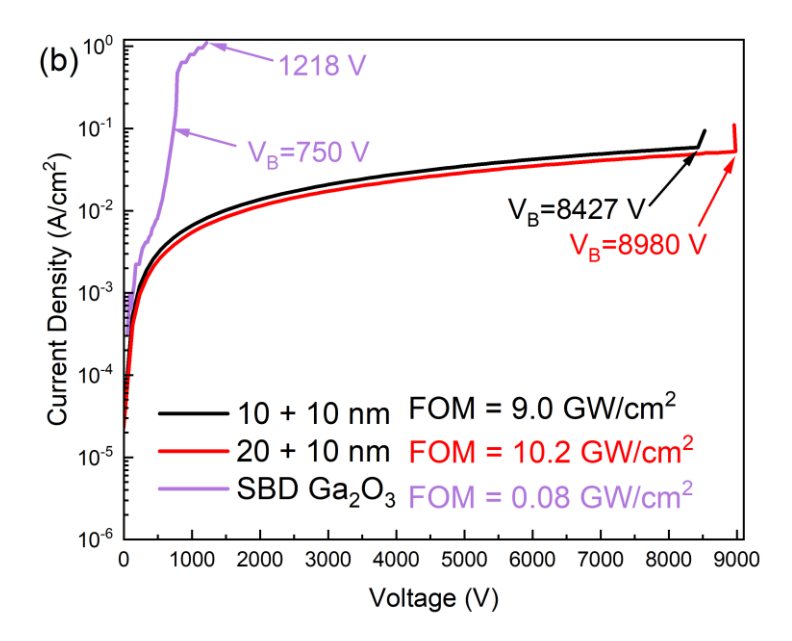


Fig. 7. (a). Reverse current characteristics from Schottky rectifier and NiO/Ga₂O₃ heterojunction rectifiers with different guard ring extensions and NiO layer thicknesses.

PLEASE CITE THIS ARTICLE AS DOI: 10.1116/6.0002722

(b) comparison between Schottky and NiO/Ga₂O₃ heterojunction rectifiers fabricated on the lowest drift layer doping wafer.

Figure 7(b) shows a comparison of the breakdown voltages for the devices fabricated on the lower drift layer doped layers, as a function of the NiO thickness. The power figure of merit was 10.2 GW.cm^{-2} for the optimized heterojunction rectifier, compared to 0.08 GW/cm^{-2} for the Schottky rectifier. The theoretical maximum is ~34 GW.cm⁻², showing that further improvement should be possible as the edge termination and epi layer quality continue to evolve $^{(4,12)}$. The average electric field strength is 8.7 MV/cm. For biases >100 V, the reverse leakage current follows a $\ln(I) \propto V$ relation. This indicates the dominant leakage mechanism is electron variable-range-hopping via defect-related states in the drift region $^{(10,12)}$. This has been reported in detail by numerous groups $^{(9,10,12,14)}$.

Figure 8 shows the on-off ratio of NiO/Ga₂O₃ heterojunction rectifiers in which the bias was switched from 5V forward to the reverse voltage shown on the x-axis. For comparison, the results for s Schottky rectifier fabricated on the same wafer are included. The values are still >10¹¹ when switching to 100V and approximately two orders of magnitude higher than that of the Schottky rectifier over this bias range. This again emphasizes an advantage of the p-n heterojunction in achieving excellent rectification characteristics.

Figure 9 shows the reverse recovery switching waveform when switching from 50 mA forward current to -10V for heterojunction rectifiers with (a) 10/10 nm or (b) 10/20 nm bilayers as a function of guard ring extension. The reverse recovery times are~ 21ns and are tabulated in Table 1. These measurements were made with a custom switching

PLEASE CITE THIS ARTICLE AS DOI: 10.1116/6.0002722

circuit, as described previously ⁽⁴¹⁻⁴³⁾. We used di/dt values around 2.9 A/us. Others have reported use of values in the range 100-400 A/us ^(48,63). Figure 10 shows a comparison of switching waveforms of Schottky and NiO/Ga₂O₃ heterojunction rectifiers. The relative indifference to device structure demonstrates that charge storage in the p-n junction is not a significant factor compared to the Schottky device ^(13,14). The Schottky diode had higher forward current due to lower effective barrier height.

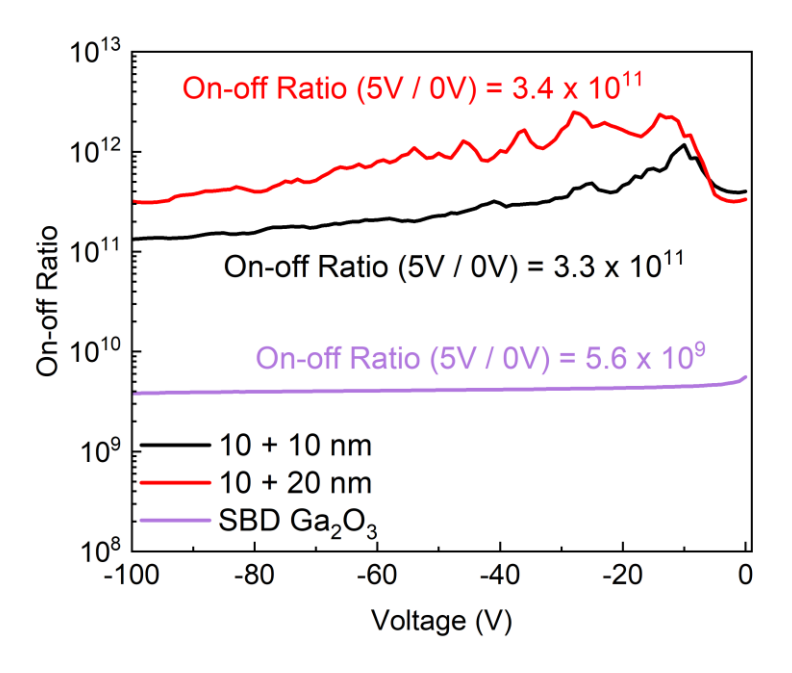


Fig. 8. On-off ratio of 100 μm diameter NiO/Ga₂O₃ heterojunction rectifiers in which the bias was switched from 5V forward to the voltage shown on the x-axis. For comparison, the results for a Schottky rectifier fabricated on the same wafer are included.

PLEASE CITE THIS ARTICLE AS DOI: 10.1116/6.0002722

(a) 80 Thickness = 10 + 10 nm GR=12 μm GR=16 μm GR=20 μm Time (ns)

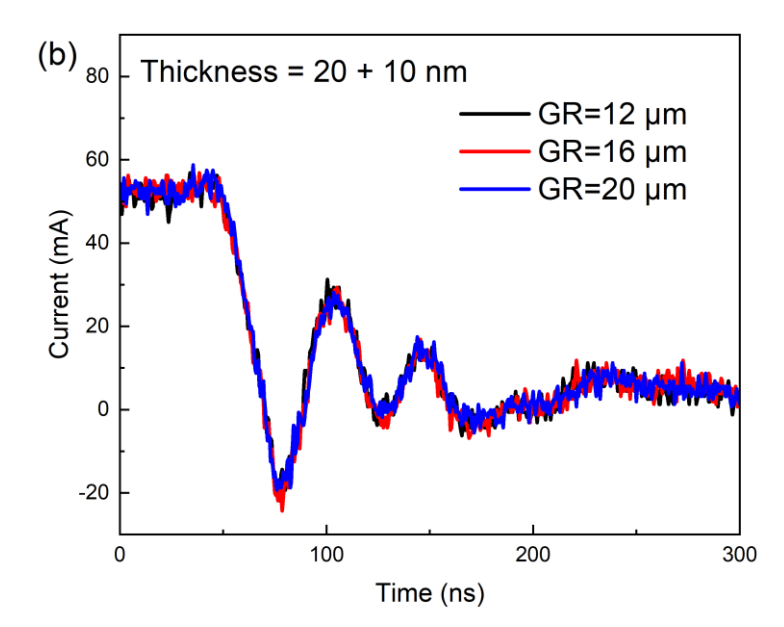


Fig. 9. (a) Switching waveform for NiO/Ga₂O₃ heterojunction rectifiers with (a) 10/10 nm or (b) 10/20 nm bilayers as a function of guard ring extension.

PLEASE CITE THIS ARTICLE AS DOI: 10.1116/6.0002722

Fig. 10. Comparison of switching waveforms of Schottky and NiO/Ga₂O₃ heterojunction rectifiers.

Table 1. Summary of reverse recovery parameters for heterojunction and Schottky rectifiers

			dI/dT (A/μs)	
10+10 nm	19.6	27.5	2.9	50
20+10 nm	13.8	21.6	2.9	50
Schottky	14.6	21.4	2.5	65

Figure 11 shows a literature compilation of Ron versus V_B results for all the common types of rectifiers fabricated in the Ga₂O₃ materials system. These include metal gate Schottky barrier or junction barrier Schottky rectifiers, along with NiO/Ga₂O₃

the online version of record will be different from this version once it has been copyedited and typeset.

PLEASE CITE THIS ARTICLE AS DOI: 10.1116/6.0002722

This is the author's peer reviewed, accepted manuscript. However,

heterojunction rectifiers. This is a standard chart for showing the improvement in Ga₂O₃ rectifier performance and contains the theoretical lines for SiC, GaN and Ga₂O₃ devices. Note that there are now at least five instances of Ga₂O₃ rectifiers with performance beyond the 1D unipolar limits of GaN and SiC. It is expected that continued optimization of the edge termination techniques and reductions in both drift layer doping and defect density should advance the ability to make large area rectifiers with high conduction currents using the NiO/ Ga₂O₃ structures. The reliability of such structures will also need to be investigated ⁽⁵²⁻⁵⁴⁾.

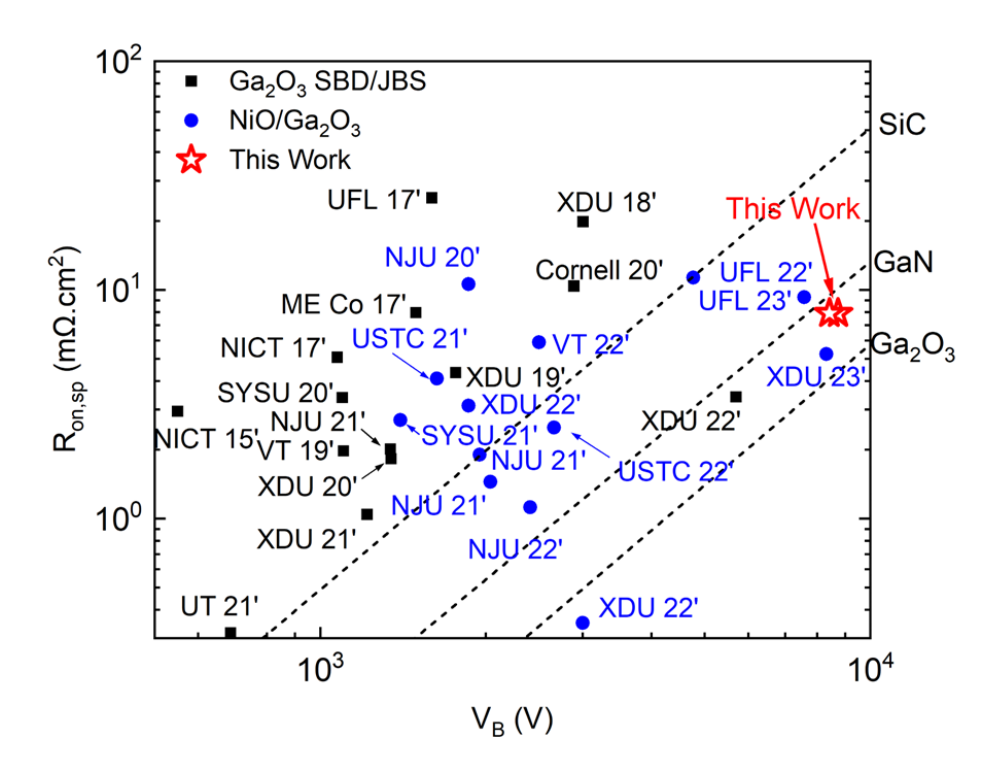


Fig. 11. Compilation of Ron versus V_B of conventional and NiO/Ga₂O₃ heterojunction small area rectifiers reported in the literature.

B. Large Area Devices to Achieve High Forward Current

PLEASE CITE THIS ARTICLE AS DOI: 10.1116/6.0002722

There has been much less reported on large area Ga₂O₃ rectifiers, which are needed to achieve large absolute forward conduction currents ^(47, 55-64). These are typically referred to as Ampere-class power devices. A recent review has discussed switching performance, packaging and approaches to thermal management ⁽⁴⁷⁾.

We fabricated 1 mm² devices with the same structure as shown in Figure 1. Figure 12 shows the forward J-V characteristics of two such devices with different NiO thicknesses, with a maximum forward current of 4.1A at 10V forward bias. The RoN values are 1.8-1.9 m Ω .cm⁻². While rectifier arrays have achieved currents in the range 33-100A, the 4A for for an individual device is still behind those of Gong et al. (48) and Zhou et al. (63), where 12A was achieved. Large area packaged Ga₂O₃ SBDs with an anode size of 3×3 mm² have been reported with forward current of over 15 A (55).

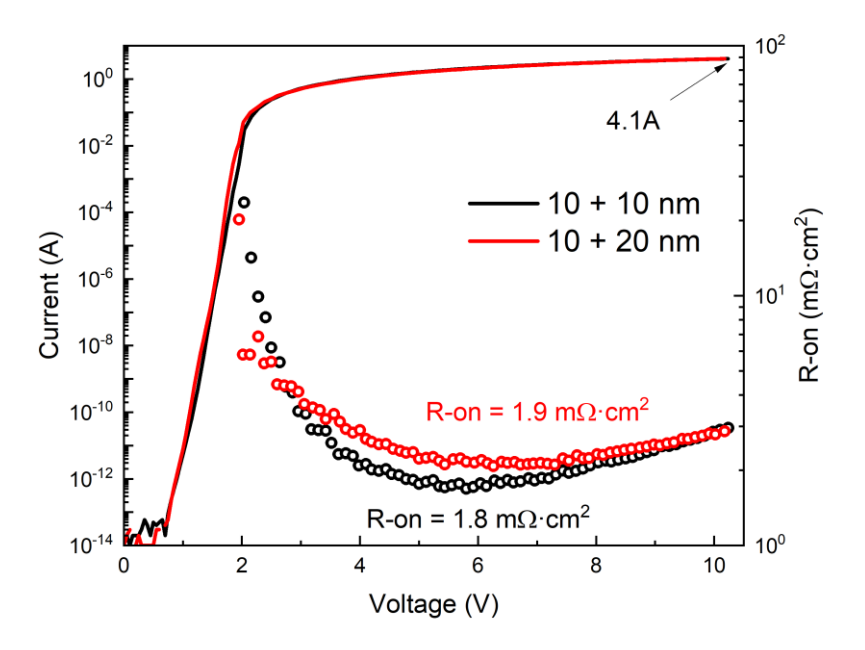


Fig. 12. Forward current characteristics for 1mm² heterojunction rectifiers for two different NiO thicknesses.

Journal of Vacuum Science & Technology A

This is the author's peer reviewed, accepted manuscript. However, the online version of record will be different from this version once it has been copyedited and typeset.

PLEASE CITE THIS ARTICLE AS DOI: 10.1116/6.0002722



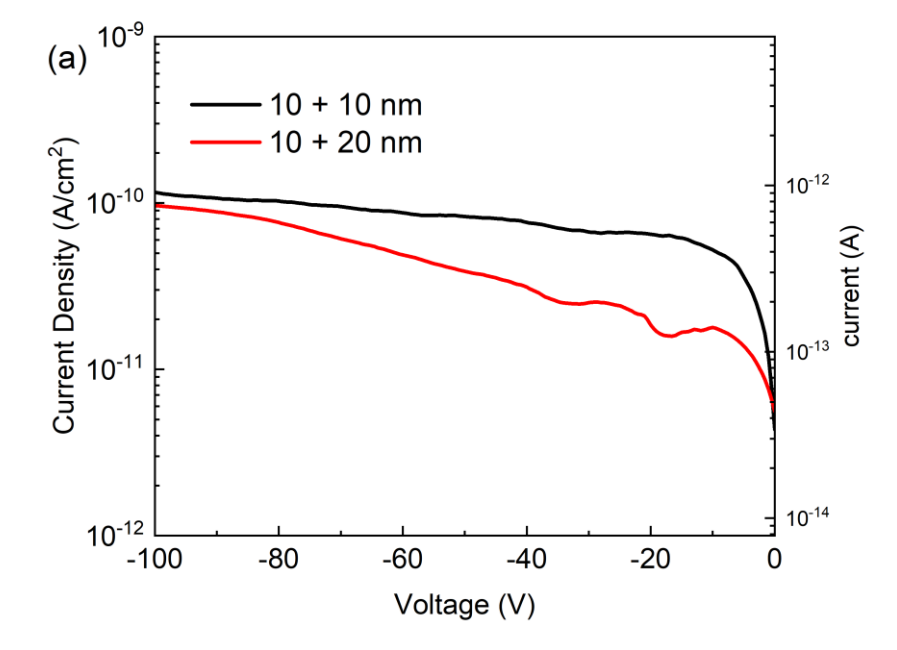
The reverse J-V characteristics are shown in Figure 13 for two different types of structure with varying NiO thickness. Figure 13 (a) shows the low voltage (-100V) range, while (b) shows the V_B values are around 4kV. These are the highest reported for impact on the magnitude of the breakdown voltage.

Ampere-class Ga₂O₃ rectifiers. Once again, the NiO thickness does not have a significant

PLEASE CITE THIS ARTICLE AS DOI: 10.1116/6.0002722

Journal of Vacuum





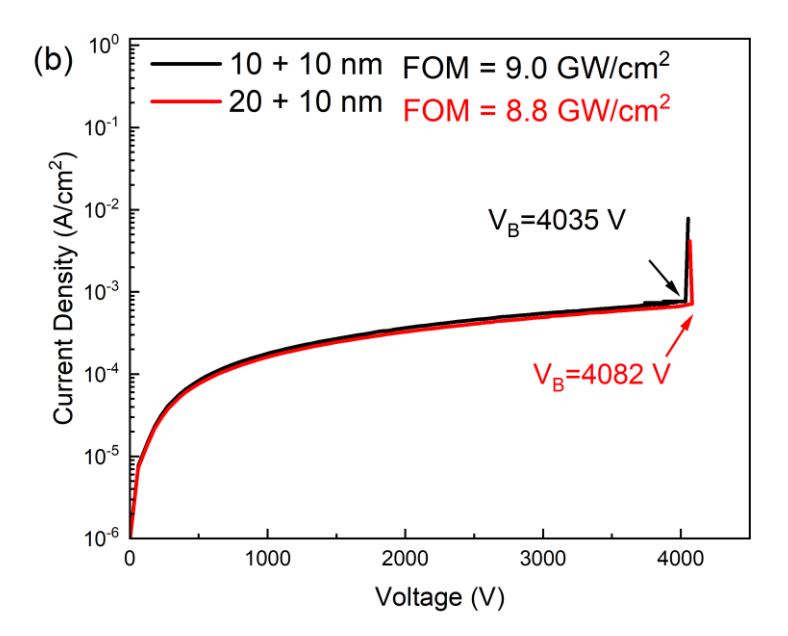


Fig. 13. Reverse J-V characteristics out to (a) -100V for NiO/Ga₂O₃ rectifiers with 10/10 nm 10/20 nm NiO bilayers. (b) over full bias range to show V_B.

Figure 14 shows the on-off ratio of 1 mm² NiO/Ga₂O₃ heterojunction rectifiers in which the bias was switched from 5V forward to the voltage shown on the x-axis. The

PLEASE CITE THIS ARTICLE AS DOI: 10.1116/6.0002722

on-off ratio is $>10^{12}\,$ over the whole bias range investigated and is slightly better for the thicker NiO layers. For switching from 10V to 0V, the ratio is $\sim 10^{14}\,$ in both cases and these large area devices retain excellent rectification, showing that the increased likelihood of having defects within the active area have not degraded this property. Sdoeung et al. $^{(65)}$ reported that threading dislocations in HVPE layers of the type we are using are responsible for significant contributions to reverse leakage current in rectifiers. Figure 15 shows a compilation of on-off ratio versus power figure of merit of conventional and NiO/Ga₂O₃ heterojunction rectifiers reported in the literature.

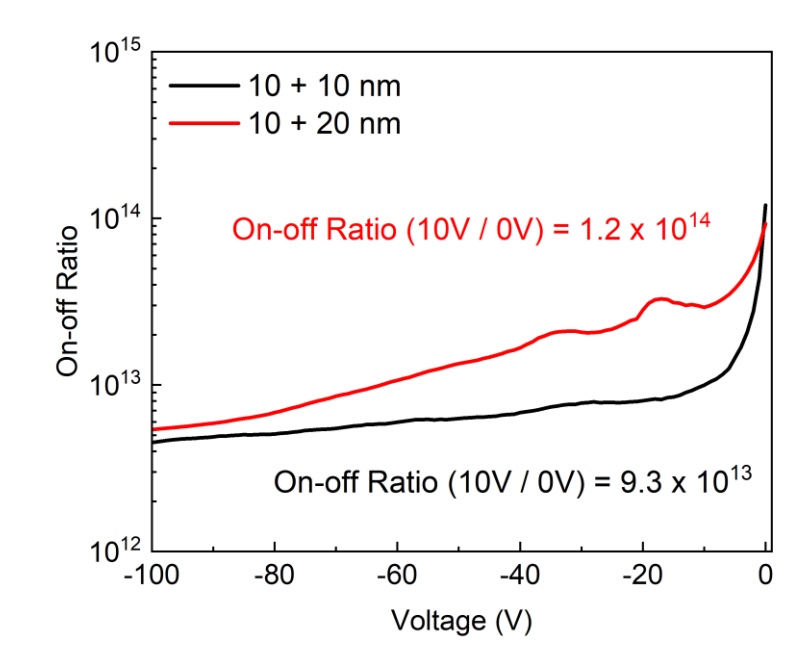


Fig. 14. On-off ratio of 1 mm² NiO/Ga₂O₃ heterojunction rectifiers in which the bias was switched from 5V forward to the voltage shown on the x-axis.

PLEASE CITE THIS ARTICLE AS DOI: 10.1116/6.0002722

10¹⁴ This Work **UFL 23'** 10^{13} **UESTC 22'** USTC 22' △ ORNL 20' 10¹² 10¹¹ ▲NJU 22' On-off Ratio XDU 20' **UFL 22'** 10¹⁰ UFL 18'▲ VT 21 UFL 19' 10⁹ Δ NCT 21' NJU 21' NJU 21' NJU 21' ▲ 10⁸ Ga₂O₃ SBD/JBS(~1mm²) 10⁷ Ga₂O₃ SBD/JBS(>1mm²) 10⁶ $NiO/Ga_2O_3(\sim 1 mm^2)$ NJU 21' This Work 10⁵ 10⁰ 10^{2} 10^{3} 10⁴ 10¹ BFOM (MW/cm²)

Fig. 15. Compilation of on-off ratio versus power figure of merit of conventional and NiO/Ga₂O₃ heterojunction rectifiers reported in the literature.

Figure 16 shows a compilation of Ron versus V_B of large area conventional and NiO/Ga₂O₃ heterojunction rectifiers reported in the literature. Our results represent the best combination of breakdown voltage and on-state resistance reported to date and show the impressive advances in material quality in terms of reducing both background carrier density and extended defect density.

PLEASE CITE THIS ARTICLE AS DOI: 10.1116/6.0002722

10^{2} ORNL 20'▲ SiC **UFL 19'** NCT 21' UFL 18' **UFL 22'** $R_{\text{on,sp}}~(m\Omega.\text{cm}^2)$ GaN 10¹ UESTC 22' ▲ Ga_2O_3 NJU 21' VT 21' NJU 22' **NJU 21** Ga₂O₃ SBD/JBS(~1mm² 10⁰ Ga₂O₃ SBD/JBS(>1mm² $NiO/Ga_2O_3(\sim 1 mm^2)$ This Work 10³ 10^2 10^{4} $V_{B}(V)$

Fig.16. Compilation of Ron versus V_B of large area conventional and NiO/Ga₂O₃ heterojunction rectifiers reported in the literature.

IV. SUMMARY AND CONCLUSIONS

In summary, we optimized the NiO bilayer thickness and extension of these layers beyond the cathode contact on NiO/ β -Ga₂O₃ p-n heterojunction rectifiers to achieve V_B 8.9 kV with R_{on} of 7.9 m Ω ·cm² and a resultant figure-of-merit (V_b²/R_{on}) of 10.2 GW.cm⁻². The heterojunction produces breakdown voltages far more than Schottky rectifiers fabricated on the same wafer and confirms that the NiO can act as both p-layer and guard ring material. This approach now consistently produces power figure of merits

PLEASE CITE THIS ARTICLE AS DOI: 10.1116/6.0002722

that exceed the unipolar power device performance of both GaN and SiC. It will still be necessary to establish the long-term reliability of devices fabricated by this approach. For large area devices, the low thermal conductivity limitations of Ga₂O₃ remain as a primary issue. In addition, more work is needed to understand the surge current capability of Ga₂O₃-based rectifiers and the packaging approaches needed to achieve practical operating characteristics, along with establishing the junction-to-ambient thermal resistance of junction side cooling approaches ⁽⁶⁶⁾.

ACKNOWLEDGMENTS

The work at UF was performed as part of Interaction of Ionizing Radiation with Matter University Research Alliance (IIRM-URA), sponsored by the Department of the Defense, Defense Threat Reduction Agency under award HDTRA1-20-2-0002. The content of the information does not necessarily reflect the position or the policy of the federal government, and no official endorsement should be inferred. The work at UF was also supported by NSF DMR 1856662.

Data Availability

The data that supports the findings of this study are available within the article.

Declarations

The authors have no conflicts to disclose.

REFERENCES

¹D M. H. Wong and M. Higashiwaki, IEEE T Electron Dev, **67**, 3925 (2020).

²X Lu, Y X Deng, Y L Pei, Z M Chen, and G Wang, Recent advances in NiO/Ga₂O₃ heterojunctions for power electronics, J. Semicond. (2023, In Press).

- ³Andrew J. Green, James Speck, Grace Xing, Peter Moens, Fredrik Allerstam, Krister Gumaelius, Thomas Neyer, Andrea Arias-Purdue, Vivek Mehrotra, Akito Kuramata, Kohei Sasaki, Shinya Watanabe, Kimiyoshi Koshi, John Blevins, Oliver Bierwagen, Sriram Krishnamoorthy, Kevin Leedy, Aaron R. Arehart, Adam T. Neal, Shin Mou, Steven A. Ringel, Avinash Kumar, Ankit Sharma, Krishnendu Ghosh, Uttam Singisetti, Wenshen Li, Kelson Chabak, Kyle Liddy, Ahmad Islam, Siddharth Rajan, Samuel Graham, Sukwon Choi, Zhe Cheng, and Masataka Higashiwaki, APL Mater. 10, 029201 (2022).
- ⁴S. J. Pearton, Fan Ren, Marko Tadjer and Jihyun Kim, J. Appl. Phys. **124**, 220901 (2018).
- ⁵Chenlu Wang, Jincheng Zhang, Shengrui Xu, Chunfu Zhang, Qian Feng, Yachao Zhang, Jing Ning, Shenglei Zhao, Hong Zhou and Yue Hao, J. Phys. D: Appl. Phys. **54**, 243001 (2021)
- ⁶Y. Kokubun, S. Kubo and S. Nakagomi Appl Phys Express, **9**, 091101 (2016).
- ⁷Yuxin Deng, Ziqi Yang, Tongling Xu, Huaxing Jiang, Kar Wei Ng, Chao Liao, Danni Su, Yanli Pei, Zimin Chen, Gang Wang, Xing Lu, Appl Surf Sci, **622**, 156917 (2023).
- ⁸Maria Isabel Pintor-Monroy, Diego Barrera, Bayron L. Murillo-Borjas, Francisco Javier Ochoa-Estrella, Julia W. P. Hsu, and Manuel A. Quevedo-Lopez, ACS Appl. Mater. Interfaces 10, 38159 (2018).
- ⁹Xinyi Xia, Jian-Sian Li, Chao-Ching Chiang, Timothy Jinsoo Yoo, Fan Ren, Honggyu Kim and S. J. Pearton, J. Phys. D: Appl. Phys. **55**, 385105 (2022).
- ¹⁰Hehe Gong, Xuanhu Chen, Yang Xu, Yanting Chen, Fangfang Ren, Bin Liu, Shulin Gu, Rong Zhang, and Jiandong Ye, IEEE T Electron Dev, **67**, 3341 (2020).
- ¹¹S. Sharma, K. Zeng, S. Saha, U. Singisetti, IEEE Electr Device L. 41, 6 836 (2020).
- ¹²Jincheng Zhang, Pengfei Dong, Kui Dang, Yanni Zhang, Qinglong Yan, Hu Xiang, Jie Su, Zhihong Liu, Mengwei Si, Jiacheng Gao, Moufu Kong, Hong Zhou and Yue Hao, Nat Commun 13, 3900 (2022).
- ¹³Pengfei Dong, Jincheng Zhang, Qinglong Yan, Zhihong Liu, Peijun Ma, Hong Zhou and Yue Hao, IEEE Electr Device L, **43**, 765 (2022).
- ¹⁴Jian-Sian Li, Chao-Ching Chiang, Xinyi Xia, Timothy Jinsoo Yoo, Fan Ren, Honggyu Kim, and S. J. Pearton, Appl. Phys. Lett. 121, 042105 (2022).

- ¹⁵S. Roy, A. Bhattacharyya, P. Ranga, H. Splawn, J. Leach and S. Krishnamoorthy, IEEE Electr Device L. 42, 1140 (2021).
- ¹⁶Arkka Bhattacharyya, Shivam Sharma, Fikadu Alema, Praneeth Ranga, Saurav Roy, Carl Peterson, Geroge Seryogin, Andrei Osinsky, Uttam Singisetti and Sriram Krishnamoorthy, Appl. Phys. Express 15, 061001(2022).
- ¹⁷K. D. Chabak, K. D. Leedy, A. J. Green, S. Mou, A. T Neal, T. Asel, E. R. Heller, N. S. Hendricks, K. Liddy, A. Crespo, N. C. Miller, M. T. Lindquist, N. Moser, R. C. Fitch Jr, D. E. Walker Jr, D. L Dorsey and G. H. Jessen, Semicond Sci Tech, 35, 013002 (2020).
- ¹⁸Zongyang Hu, Kazuki Nomoto, Wenshen Li, Zexuan Zhang, Nicholas Tanen, Quang Tu Thieu, Kohei Sasaki, Akito Kuramata, Tohru Nakamura, Debdeep Jena, and Huili Grace Xing, Appl. Phys. Lett. 113, 122103 (2018).
- ¹⁹Ribhu Sharma, Minghan Xian, Chaker Fares, Mark E. Law, Marko Tadjer, Karl D. Hobart, Fan Ren and Stephen J. Pearton, J. Vac. Sci. Technol A **39**, 013406 (2021).
- ²⁰Wenshen Li, Devansh Saraswat, Yaoyao Long, Kazuki Nomoto, Debdeep Jena, and Huili Grace Xing, Appl. Phys. Lett. **116**, 192101 (2020).
- ²¹Y. Lv, Y. Wang, X. Fu, Shaobo Dun, Z. Sun, Hongyu Liu, X. Zhou, X. Song, K. Dang, S. Liang, J. Zhang, H. Zhou, Z. Feng, S. Cai and Yue Hao, IEEE T Power Electr. **36**, 6179 (2021).
- ²²C. Liao, Xing Lu, Tongling Xu, Paiwen Fang, Yuxin Deng, Haoxun Luo, Zhisheng Wu, Zimin Chen, Jun Liang, Yanli Pei and Gang Wang, IEEE T Electron Dev, 69, 5722 (2022).
- ²³Ming Xiao, Boyan Wang, Jingcun Liu, Ruizhe Zhang, Zichen Zhang, Chao Ding, Shengchang Lu, Kohei Sasaki, Guo-Quan Lu, Cyril Buttay and Yuhao Zhang, IEEE T Power Electr 36, 8565 (2021).
- ²⁴X. Lu, Xianda Zhou, Huaxing Jiang, Kar Wei Ng, Zimin Chen, Yanli Pei, Kei May Lau and Gang Wang, IEEE Electr Device L.**41**, 449 (2020).
- ²⁵Chenlu Wang, Hehe Gong, Weina Lei, Y. Cai, Z. Hu, Shengrui Xu, Zhihong Liu, Qian Feng, Hong Zhou, Jiandong Ye, Jincheng Zhang, Rong Zhang, and Yue Hao, IEEE Electr Device L, **42**, 485 (2021).
- ²⁶Qinglong Yan, Hehe Gong, Jincheng Zhang, Jiandong Ye, Hong Zhou, Zhihong Liu, Shengrui Xu, Chenlu Wang, Zhuangzhuang Hu, Qian Feng, Jing Ning, Chunfu Zhang, Peijun Ma, Rong Zhang, and Yue Hao, Appl. Phys. Lett. 118, 122102 (2021).

- ²⁷H. H. Gong, X. H. Chen, Y. Xu, F.-F. Ren, S. L. Gu and J. D. Ye, Appl. Phys. Lett., **117**, 022104 (2020).
- ²⁸Hehe Gong, Feng Zhou, Weizong Xu, Xinxin Yu, Yang Xu, Yi Yang, Fang-fang Ren, Shulin Gu, Youdou Zheng, Rong Zhang, Hai Lu and Jiandong Ye, IEEE T Power Electr., **36**, 12213 (2021).
- ²⁹H. H. Gong, X. X. Yu, Y. Xu, X. H. Chen, Y. Kuang, Y. J. Lv, Y. Yang, F.-F. Ren, Z. H. Feng, S. L. Gu, Y. D. Zheng, R. Zhang, and J. D. Yue, Appl. Phys. Lett. 118, 202102 (2021).
- ³⁰W. Hao, Q. He, K. Zhou, G. Xu, W. Xiong, X. Zhou, G. Jian, C. Chen, X. Zhao, and S. Long, Appl. Phys. Lett., 118, 043501 (2021).
- ³¹F. Zhou, Hehe Gong, Weizong Xu, Xinxin Yu, Yang Xu, Yi Yang, Fang-fang Ren, Shulin Gu, Youdou Zheng, Rong Zhang, Jiandong Ye and Hai Lu, IEEE T Power Electr, **37**, 1223 (2022).
- ³²Qinglong Yan, Hehe Gong, Hong Zhou, Jincheng Zhang, Jiandong Ye, Zhihong Liu, Chenlu Wang, Xuefeng Zheng, Rong Zhang, and Yue Hao, Appl. Phys. Lett. 120, 092106 (2022).
- ³³Y. J. Lv, Y. G. Wang, X. C. Fu, S. B. Dun, Z. F. Sun, H. Y. Liu, X. Y. Zhou, X. B. Song, K. Dang, S. X. Liang, J. C. Zhang, H. Zhou, Z. H. Feng, S. J. Cai, and Y. Hao, IEEE T Power Electron. 36, 6179 (2021).
- ³⁴Jiaye Zhang, Shaobo Han, Meiyan Cui, Xiangyu Xu, Weiwei Li, Haiwan Xu, Cai Jin, Meng Gu, Lang Chen and Kelvin H. L. Zhang, ACS Appl. Electron. Mater. 2, 456 (2020).
- ³⁵Yuangang Wang, Hehe Gong, Yuanjie Lv, Xingchang Fu, Shaobo Dun, Tingting Han, Hongyu Liu, Xingye Zhou, Shixiong Liang, Jiandong Ye, Rong Zhang, Aimin Bu, Shujun Cai and Zhihong Feng, IEEE T Power Electr. 37, 3743 (2022).
- ³⁶Hong Zhou, Shifan Zeng, Jincheng Zhang, Zhihong Liu, Qian Feng, Shengrui Xu, Jinfeng Zhang and Yue Hao, Crystals 11, 1186 (2021).
- ³⁷Zhengpeng Wang, Hehe Gong, Chenxu Meng, Xinxin Yu, Xinyu Sun, Chongde Zhang, Xiaoli Ji, Fangfang Ren, Shulin Gu, Youdou Zheng, Rong Zhang, and Jiandong Ye, IEEE T Electron Dev, 69, 981 (2022).
- ³⁸Boyan Wang, Ming Xiao, Joseph Spencer, Yuan Qin, Kohei Sasaki, Marko J. Tadjer and Yuhao Zhang, IEEE Electr Device L **44**, 221 (2023).

- ³⁹F. Zhou, H. H. Gong, Z. P. Wang, W. Z. Xu, X. X. Yu, Y. Yang, F.-F. Ren, S. L. Gu, R. Zhang, Y. D. Zheng, H. Lu, and J. D. Ye, Appl. Phys. Lett. 119, 262103 (2021)
- ⁴⁰Jiancheng Yang, Minghan Xian, Patrick Carey, Chaker Fares, Jessica Partain, Fan Ren, Marko Tadjer, Elaf Anber, Dan Foley, Andrew Lang, James Hart, James Nathaniel, Mitra L. Taheri, S. J. Pearton and Akito Kuramata, Appl. Phys. Lett. 114, 232106 (2019).
- ⁴¹J. Yang, F. Ren, Y.-T. Chen, Y.-T. Liao, C.-W. Chang, J. Lin, M. J. Tadjer, S. J. Pearton, and A. Kuramata, IEEE J. Electron Devi., 7, 57 (2019).
- ⁴²Yen-Ting Chen, Jiancheng Yang, Fan Ren, Chin-Wei Chang, Jenshan Lin, S.J. Pearton, Marko J Tadjer, Akito Kuramata and Yu-Te Liao, ECS J. Solid State SC **8**, Q3229 (2019).
- ⁴³Jian-Sian Li, Chao-Ching Chiang, Xinyi Xia, Fan Ren and S. J. Pearton, J. Vac Sci Technol A **40**, 063407 (2022).
- ⁴⁴W. Hao, Q. He, X. Zhou, X. Zhao, G. Xu and S. Long, "2.6 kV NiO/Ga₂O₃ Heterojunction Diode with Superior High-Temperature Voltage Blocking Capability," 2022 IEEE 34th International Symposium on Power Semiconductor Devices and ICs (ISPSD), Vancouver, BC, Canada, 2022, pp. 105-108.
- ⁴⁵ Weibing Hao, Feihong Wu, Wenshen Li, Guangwei Xu, Xuan Xie, Kai Zhou, Wei Guo, Xuanze Zhou, Qiming He, Xiaolong Zhao, Shu Yang and Shibing Long, "High-Performance Vertical β-Ga₂O₃ Schottky Barrier Diodes Featuring P-NiO JTE with Adjustable Conductivity," 2022 International Electron Devices Meeting (IEDM), San Francisco, CA, USA, 2022, pp. 9.5.1-9.5.4.
- ⁴⁶ X. Zhou, Q. Liu, W. Hao, G. Xu and S. Long, "Normally-off β-Ga₂O₃ Power Heterojunction Field-Effect-Transistor Realized by p-NiO and Recessed-Gate," 2022 IEEE 34th International Symposium on Power Semiconductor Devices and ICs (ISPSD), Vancouver, BC, Canada, 2022, pp. 101-104.
- ⁴⁷Yuan Qin, Zhengpeng Wang, Kohei Sasaki, Jiandong Ye and Yuhao Zhang, Jpn J. Appl Phys **62**, SF0801 (2023).
- ⁴⁸H. Gong, F. Zhou, W. Xu, X. Yu, Y. Xu, Y. Yang, F. Ren, S. Gu, Y. Zheng and R. Zhang, IEEE T Power Electr, **36**, 12213 (2021).
- ⁴⁹J. Yang, F. Ren, M. Tadjer, S.J. Pearton and A. Kuramata AIP Advances, 8.055026 (2018).
- ⁵⁰J. Yang, C. Fares, R. Elhassani, M. Xian, F. Ren, S.J. Pearton, M. Tadjer and A. Kuramata, ECS J Solid State SC, 8, Q3159 (2019).

- ⁵¹M. Ji, N.R. Taylor, I. Kravchenko, P. Joshi, T. Aytug, L.R. Cao and M.P. Paranthaman, IEEE T Power Electr, **36**, 41 (2020).
- ⁵²Zahabul Islam, Aman Haque, Nicholas Glavin, Minghan Xian, Fan Ren, Alexander Y.
 Polyakov, Anastasia Kochkova, Marko Tadjer and S.J. Pearton, ECS J. Solid State SC.9, 055008 (2020).
- ⁵³Z. Islam, M. Xian, A. Haque, F. Ren, M. Tadjer and S.J. Pearton, IEEE T. Electro Dev. 67, 3056 (2020).
- ⁵⁴Rujun Sun, Andrew R. Balog, Haobo Yang, Nasim Alem, Michael A. Scarpulla, IEEE Electron Device L (in press, 2023).
- ⁵⁵M. Xiao, B. Wang, J. Liu, R. Zhang, R. Zhang, C. Ding, S. Lu, K. Sasaki, G.Q. Lu, C. Buttay and Y. Zhang, IEEE T Power Electr 36, 8565 (2021).
- ⁵⁶H. Gong, F. Zhou, X. Yu, W. Xu, F. Ren, S. Gu, H. Lu, J. Ye. and R. Zhang, IEEE Electr Device L, 43,773 (2022).
- ⁵⁷F. Otsuka, H. Miyamoto, A. Takatsuka, S. Kunori, K. Sasaki and A. Kuramata, A., Appl Phys Express, **15**, 016501 (2021).
- ⁵⁸Jiancheng Yang, Minghan Xian, Patrick Carey, Chaker Fares, Jessica Partain, Fan Ren, Marko Tadjer, Elaf Anber, Dan Foley, Andrew Lang, James Hart, James Nathaniel, Mitra L. Taheri, S. J. Pearton and Akito Kuramata, Appl. Phys. Lett. **114**, 232106 (2019).
- ⁵⁹ W. Hao, F. Wu, W. Li, G. Xu, X. Xie, K. Zhou, W. Guo, X. Zhou, Q. He, X. Zhao and S. Yang, 2022, December. High-Performance Vertical β-Ga₂ O₃ Schottky Barrier Diodes Featuring P-NiO JTE with Adjustable Conductivity. In 2022 International Electron Devices Meeting (IEDM) (pp. 9-5). IEEE.
- ⁶⁰Y. Lv, Y. Wang, X. Fu, S. Dun, Z. Sun, H. Liu, X. Zhou, X. Song, K. Dang, S. Liang. and J. Zhang, IEEE T Power Electr, 3, .6179 (2020).
- ⁶¹J. Wei, Y. Wei, J. Lu, X. Peng, Z. Jiang, K. Yang and X. Luo, 2022, May. Experimental Study on Electrical Characteristics of Large-Size Vertical β-Ga₂O₃ Junction Barrier Schottky Diodes. In 2022 IEEE 34th International Symposium on Power Semiconductor Devices and ICs (ISPSD) (pp. 97-100). IEEE.
- ⁶²F. Zhou, H.H. Gong, Z.P. Wang, W.Z. Xu, X.X. Yu, Y.Yang, F.F. Ren, S.L. Gu, R. Zhang, Y.D. Zheng and H. Lu, Appl Phys Lett, 119, 262103 (2021).

PLEASE CITE THIS ARTICLE AS DOI: 10.1116/6.0002722

- ⁶³F. Zhou, H. Gong, W. Xu, X. Yu, Y. Xu, Y. Yang, F.F. Ren, S. Gu, Y. Zheng, R. Zhang, and J. Ye, J., IEEE T Power Electr, 37,1223 (2021).
- ⁶⁴J.S. Li, C.C. Chiang, X. Xia, C.T. Tsai, F. Ren, Y.T. Liao and S.J. Pearton, ECS J Solid State SC, **11**.105003 (2022).
- ⁶⁵Sayleap Sdoeung, Kohei Sasaki, Katsumi Kawasaki, Jun Hirabayashi, Akito Kuramata and Makoto Kasu, Jpn. J Appl Phys 62, SF1001 (2023).
- ⁶⁶B. Wang, Ming Xiao, Jack Knoll, Cyril Buttay, Kohei Sasaki, Christina Dimarino and Yuhao Zhang, IEEE Electr Device L, 42, 1132 (2021).

Journal of Vacuum Science & Technology



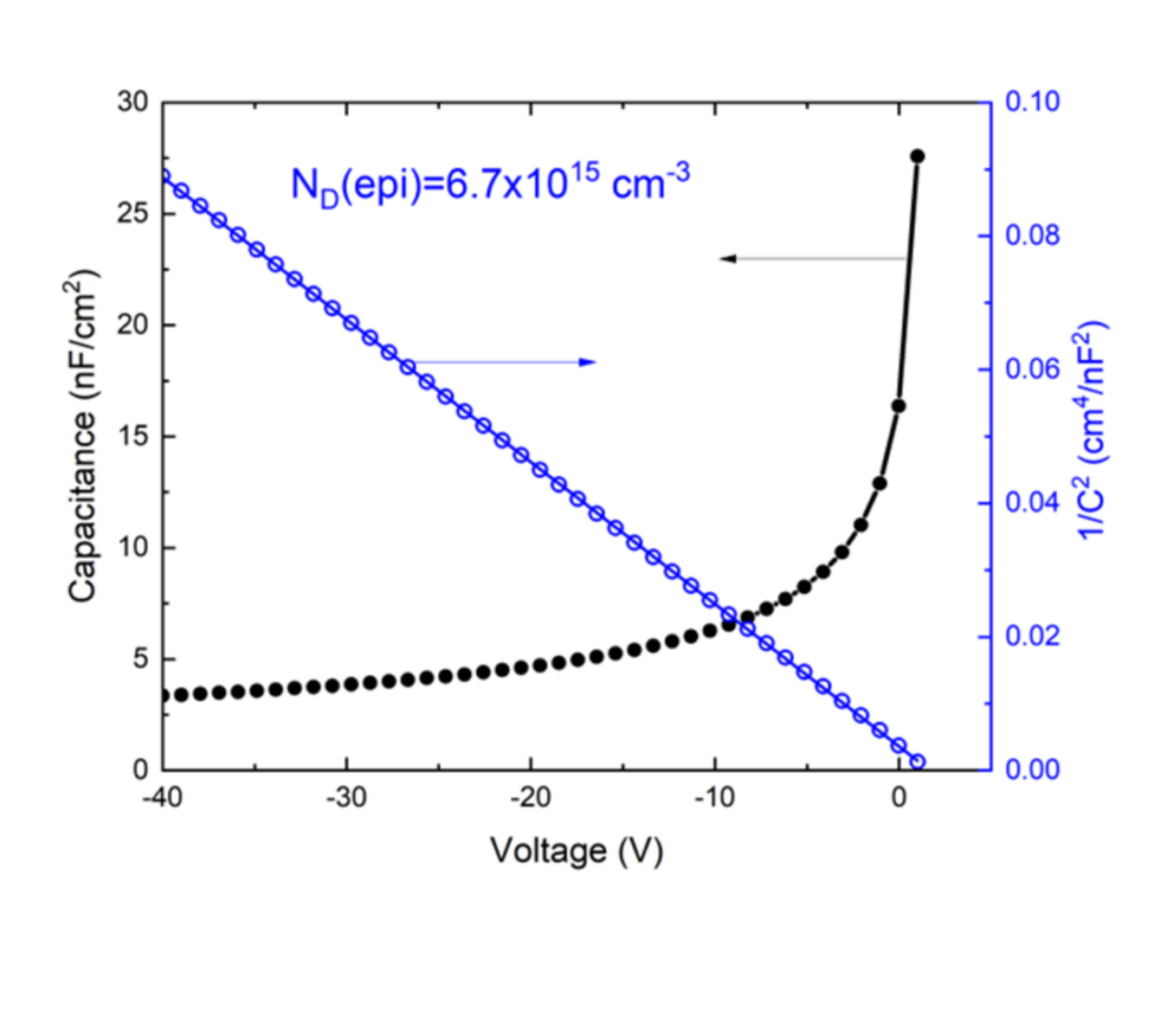
This is the author's peer reviewed, accepted manuscript. However, the online version of record will be different from this version once it has been copyedited and typeset.

PLEASE CITE THIS ARTICLE AS DOI: 10.1116/6.0002722

| 100 μm | GR = 12, 16, 20 μm | Ni/Au | NiO (10 nm) | p- = 2.6x10¹⁸ cm⁻³ | NiO (10 or 20 nm) | p- = 1.0x10¹⁸ cm⁻³ | Si-doped Ga₂O₃ (10μm) | n- = 6.7x10¹⁵ cm⁻³ | Sn-doped Ga₂O₃ (650μm) | n+ = 8x10¹⁸ cm⁻³ | Ti/Au

Journal of Vacuum Science & Technology

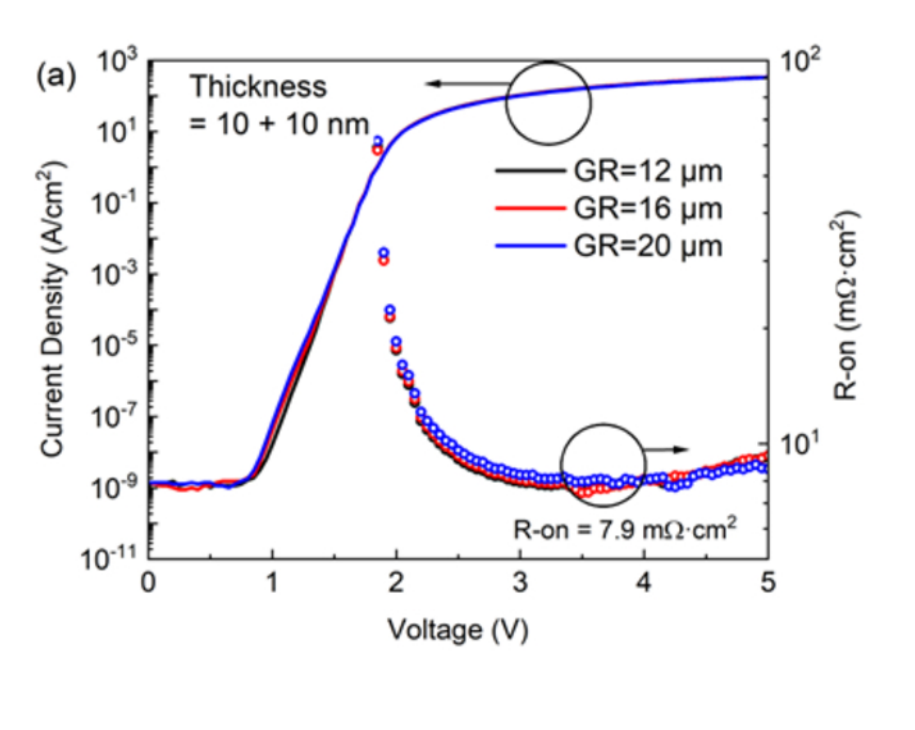


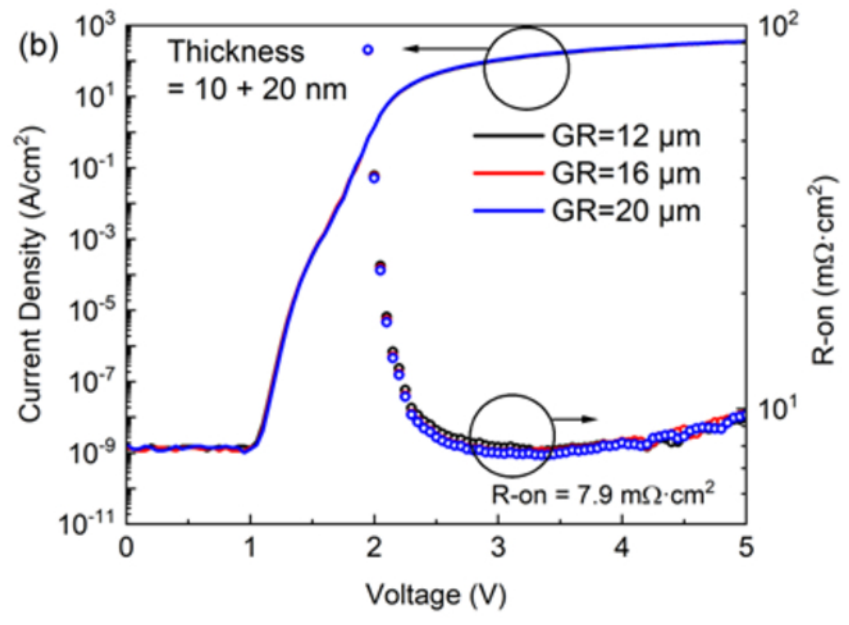




Journal of Vacuum Science & Technology A

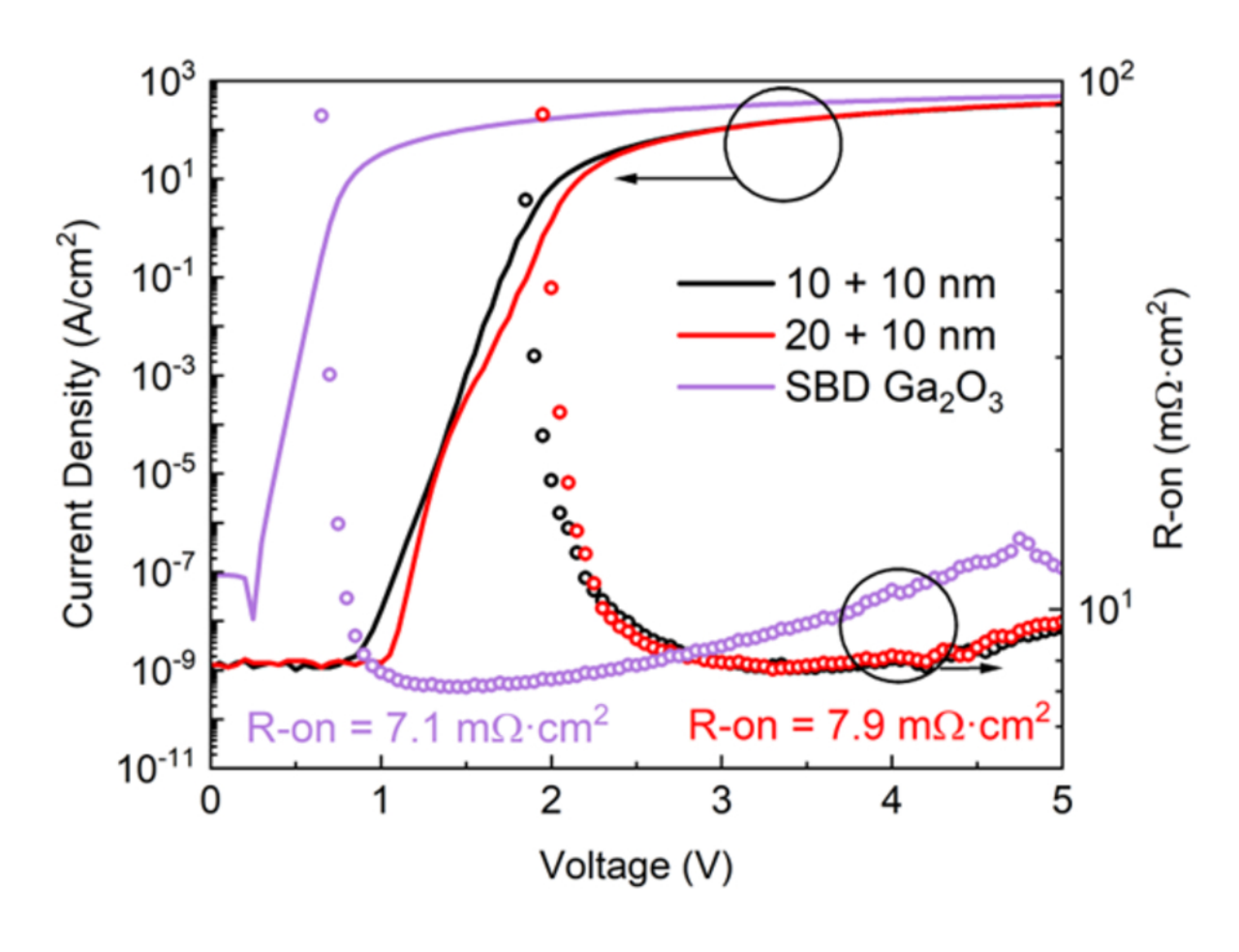
ACCEPTED MANUSCRIPT





Technology A Journal of Vacuum Science

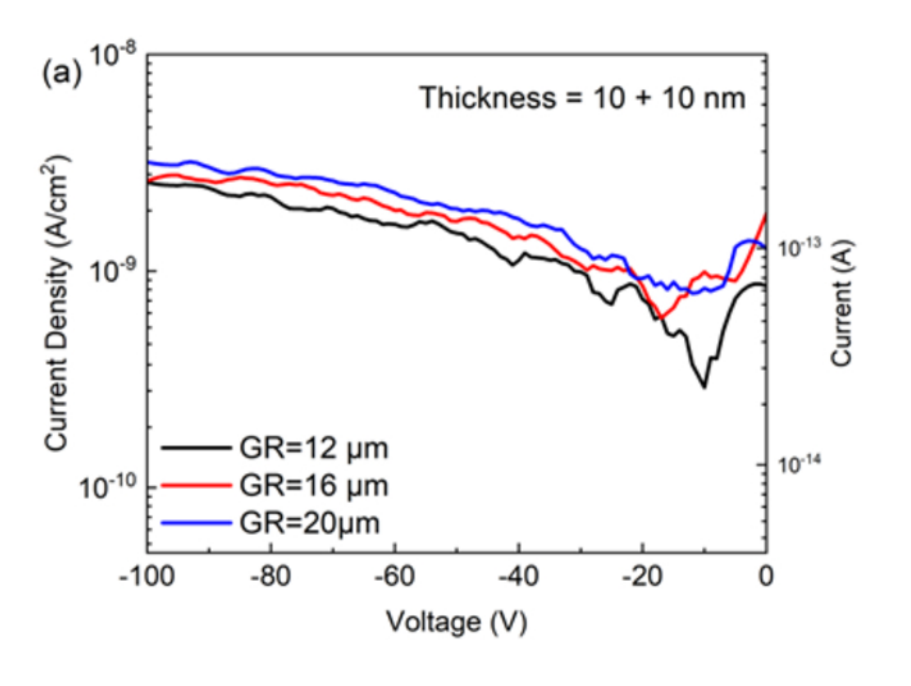


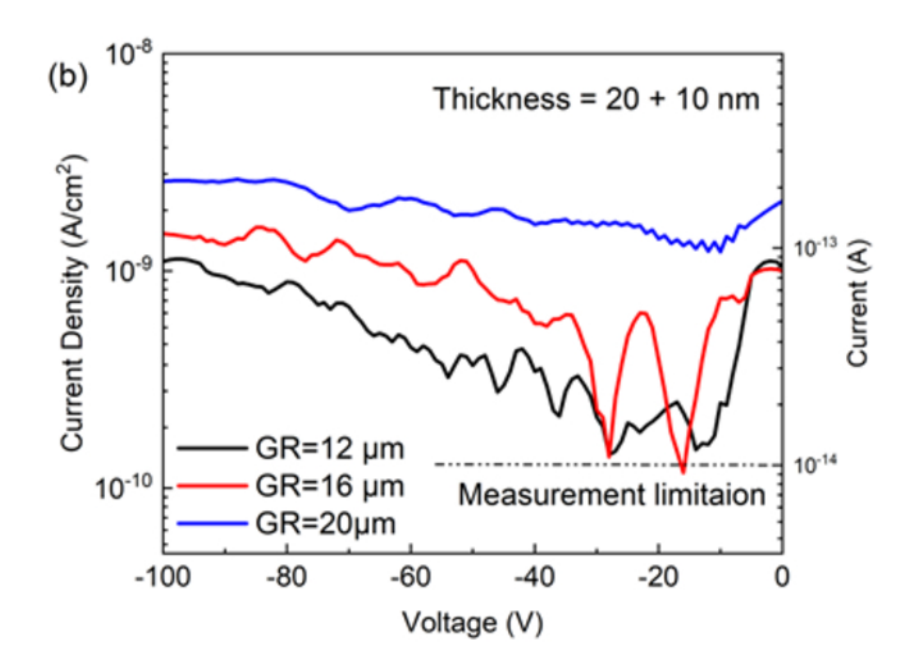


Technology A Vacuum Science Journal

ACCEPTED MANUSCRIPT

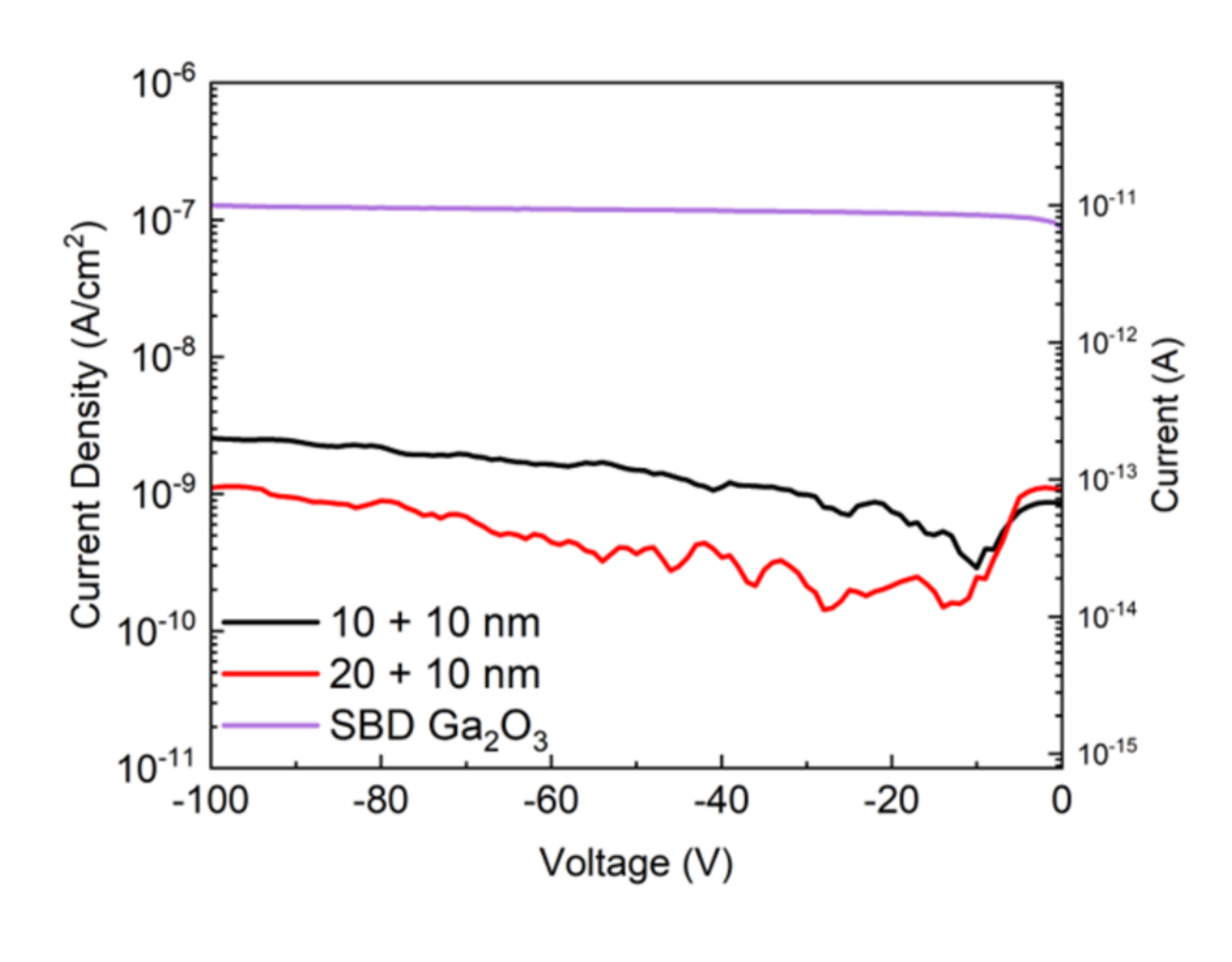






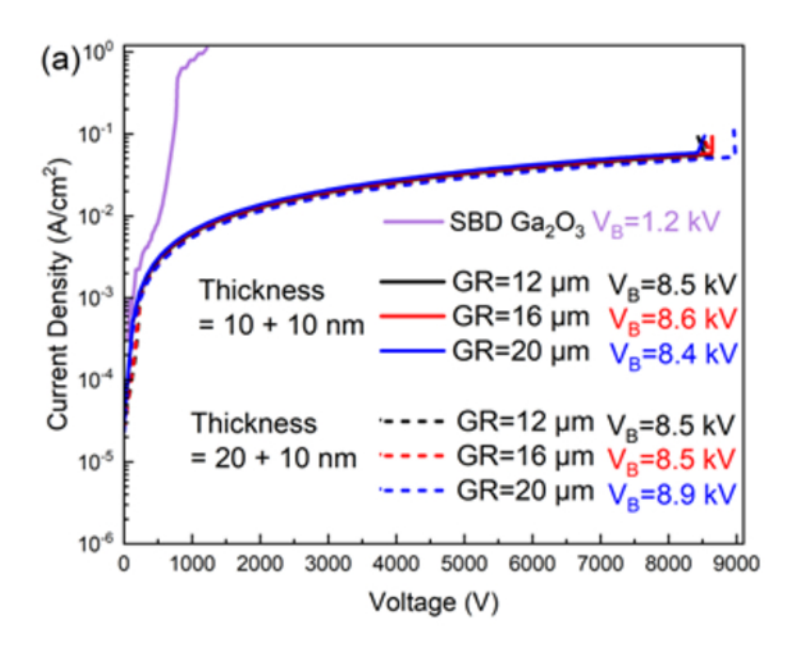
Technology A Vacuum Journal of Science

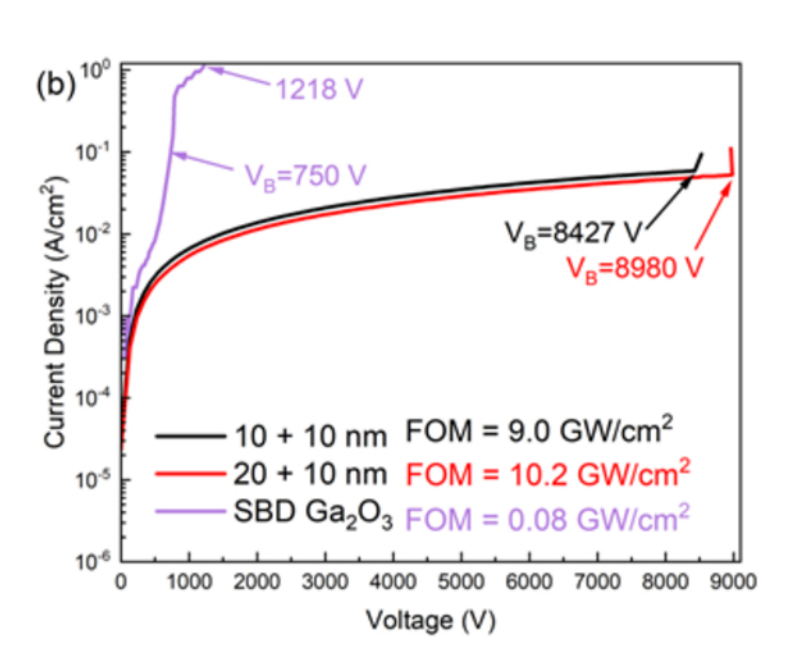




Technology A Vacuum Science Journal

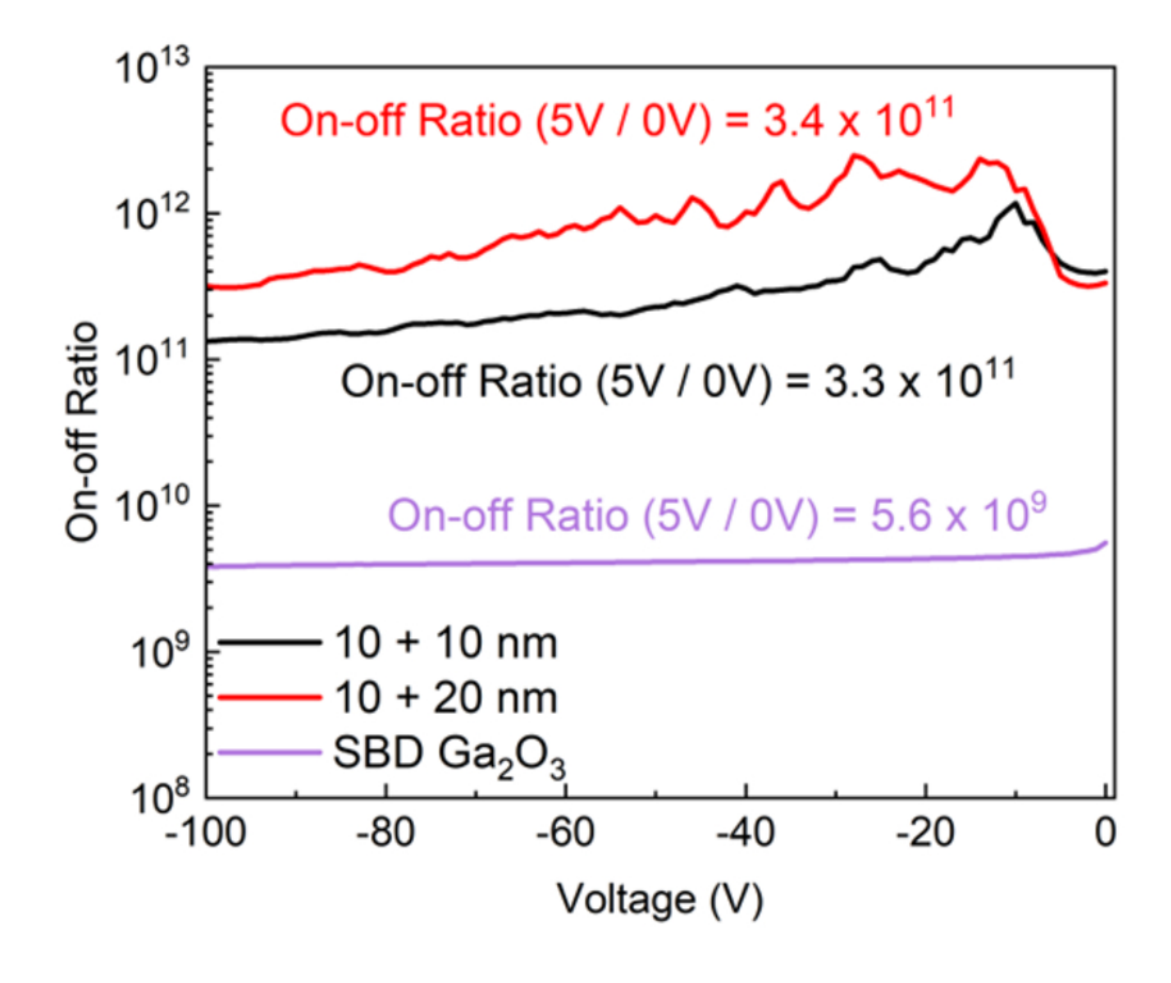






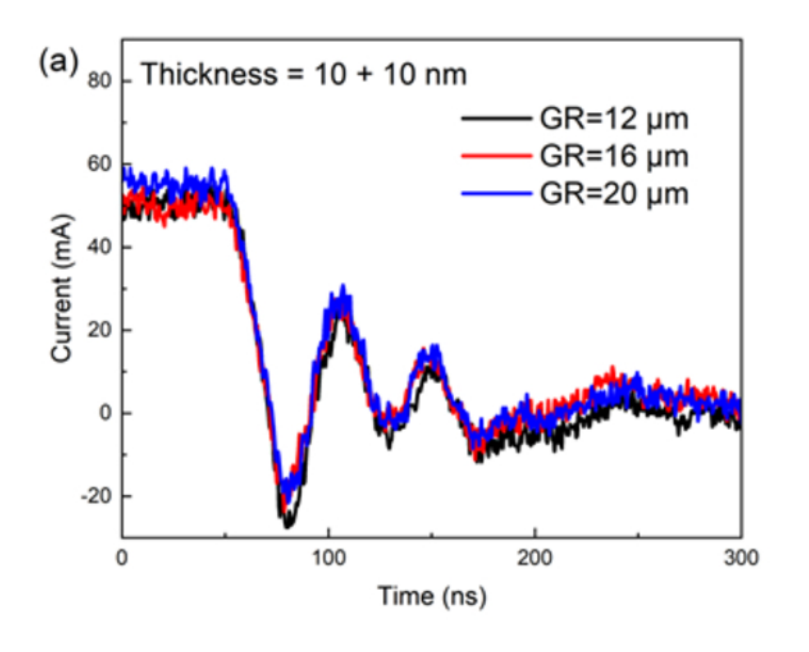
Journal of Vacuum Science & Technology

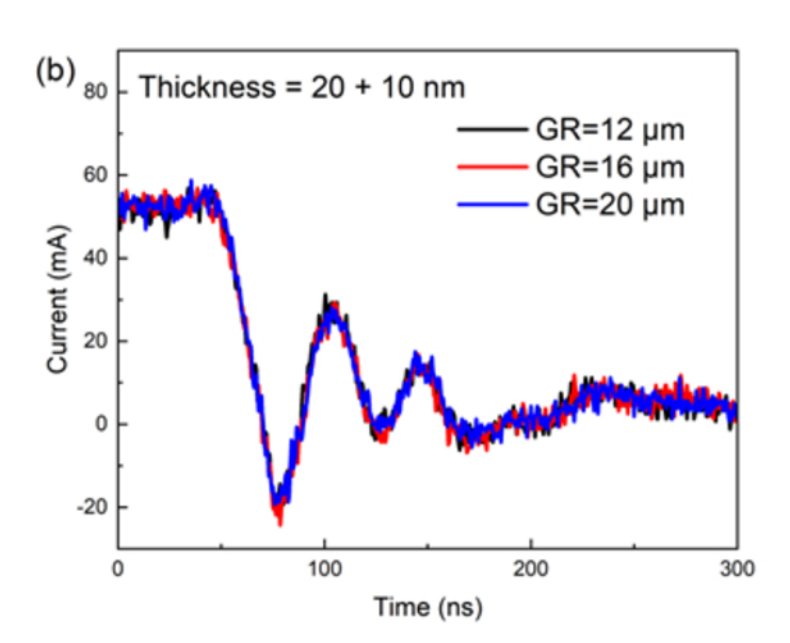




Technology A Journal of Vacuum Science

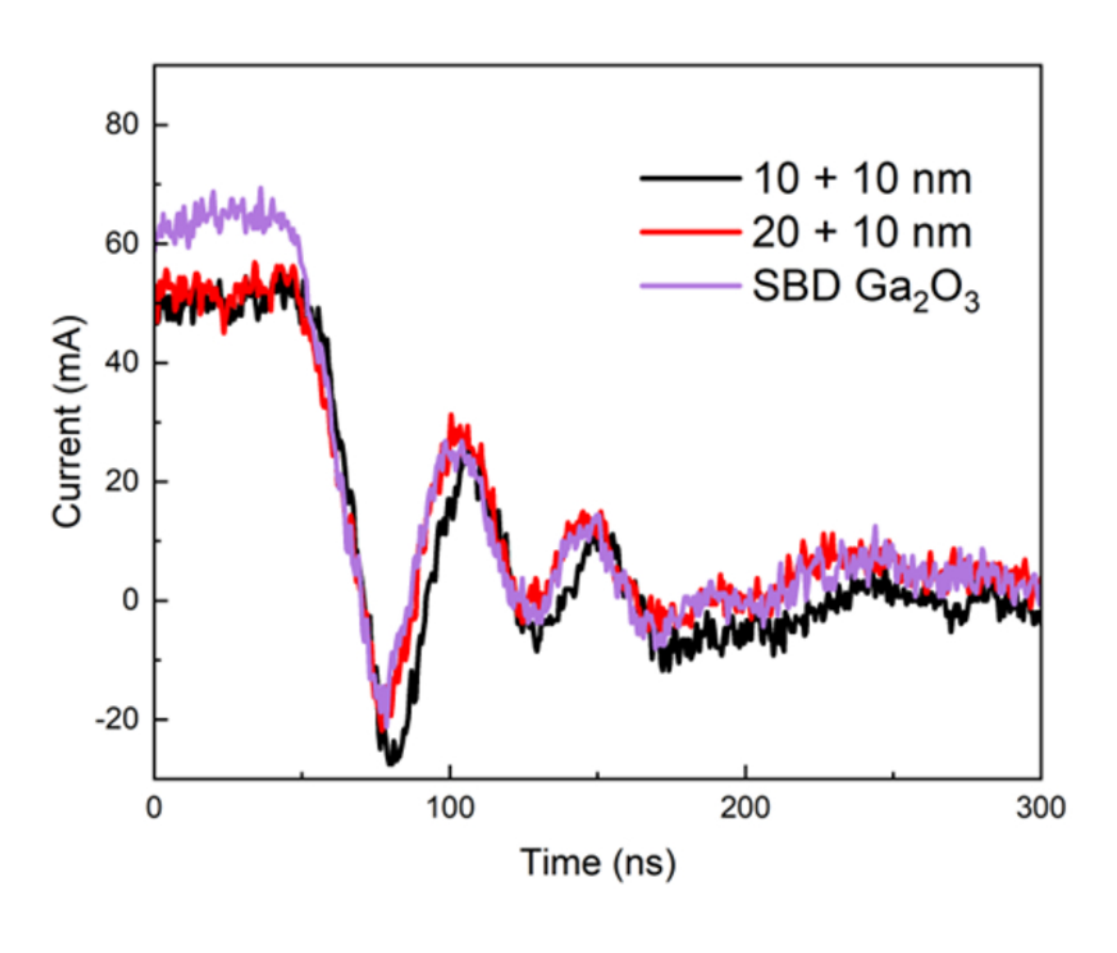






Technology A Journal of Vacuum Science &



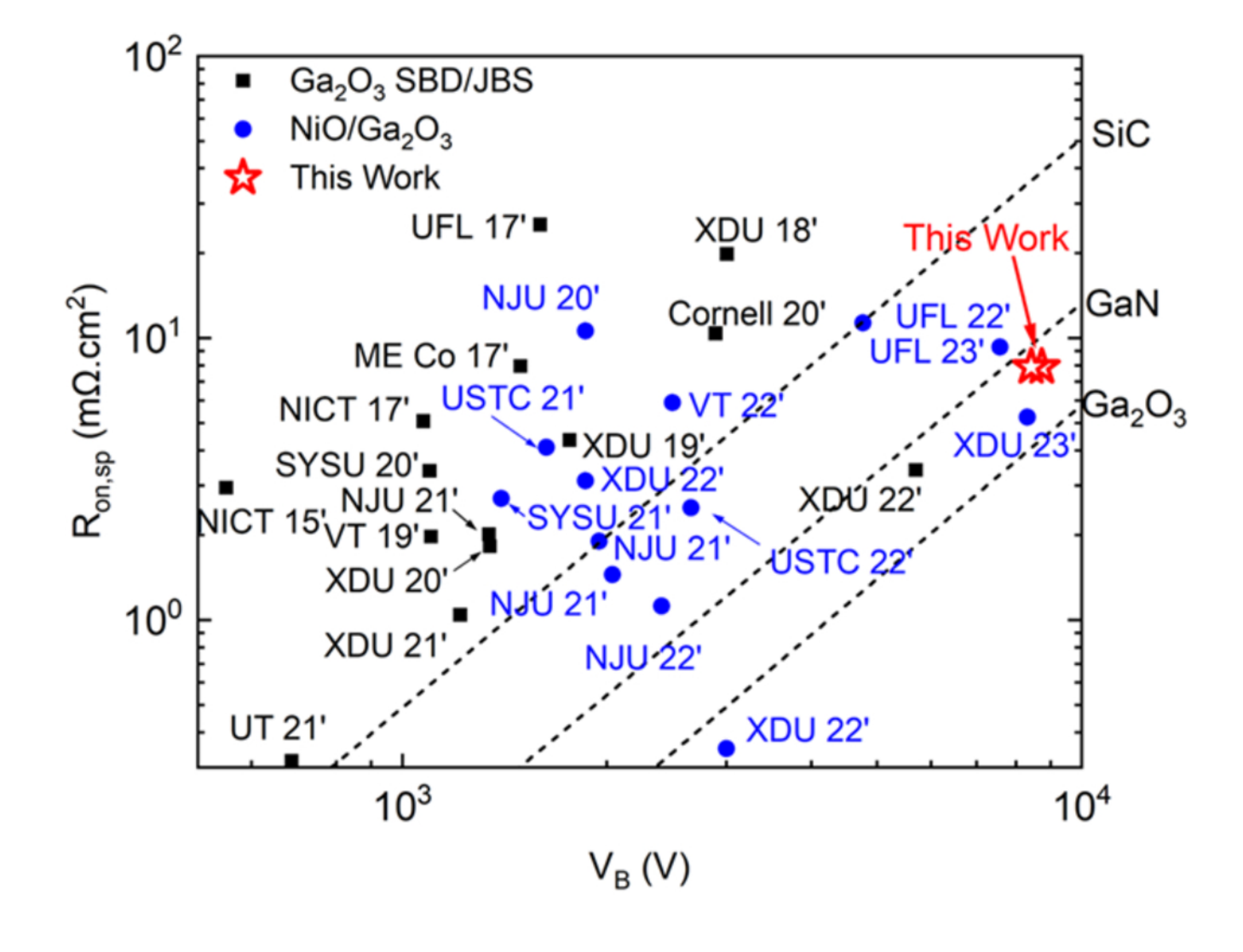


Journal of Vacuum Science & Technology



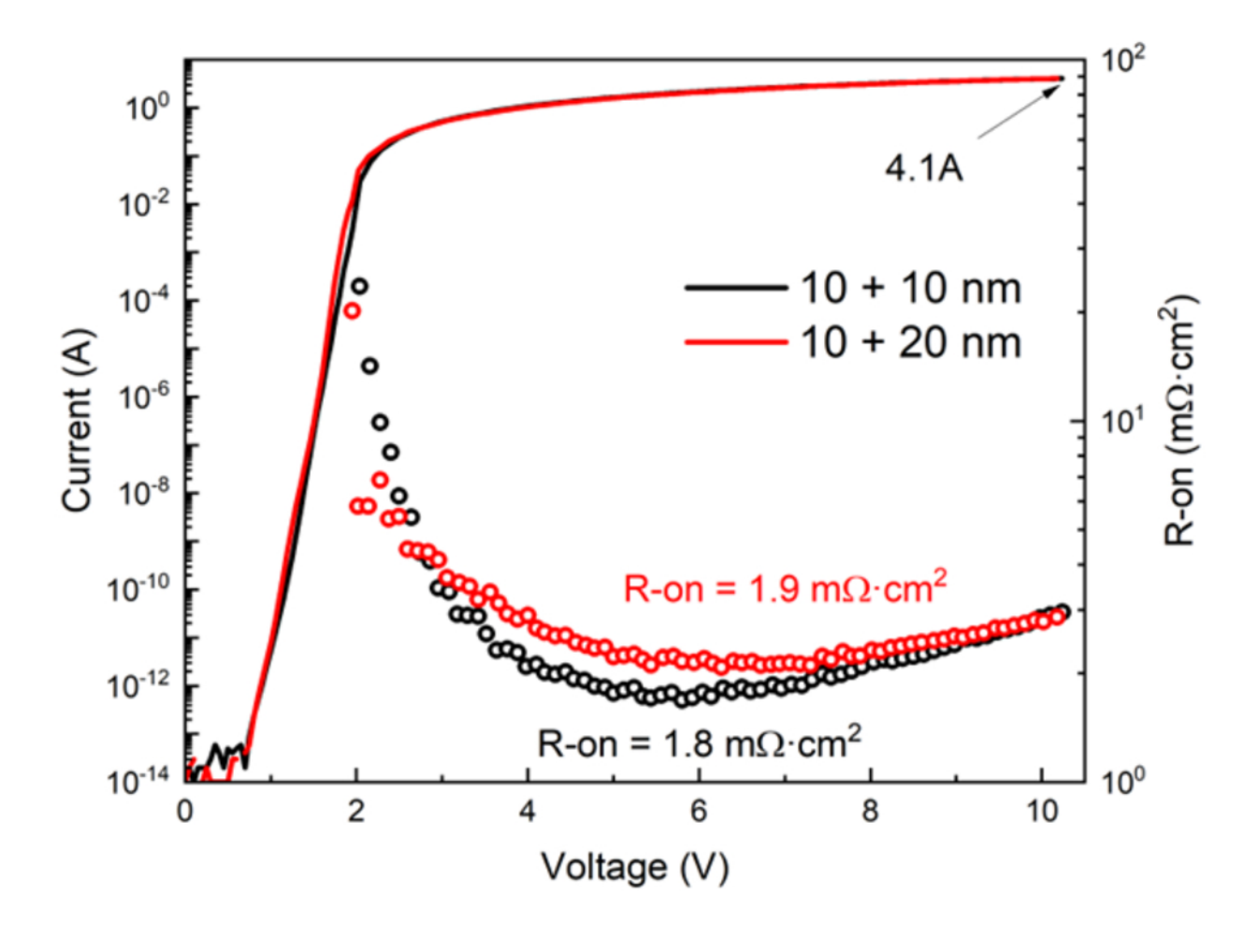
This is the author's peer reviewed, accepted manuscript. However, the online version of record will be different from this version once it has been copyedited and typeset.

PLEASE CITE THIS ARTICLE AS DOI: 10.1116/6.0002722



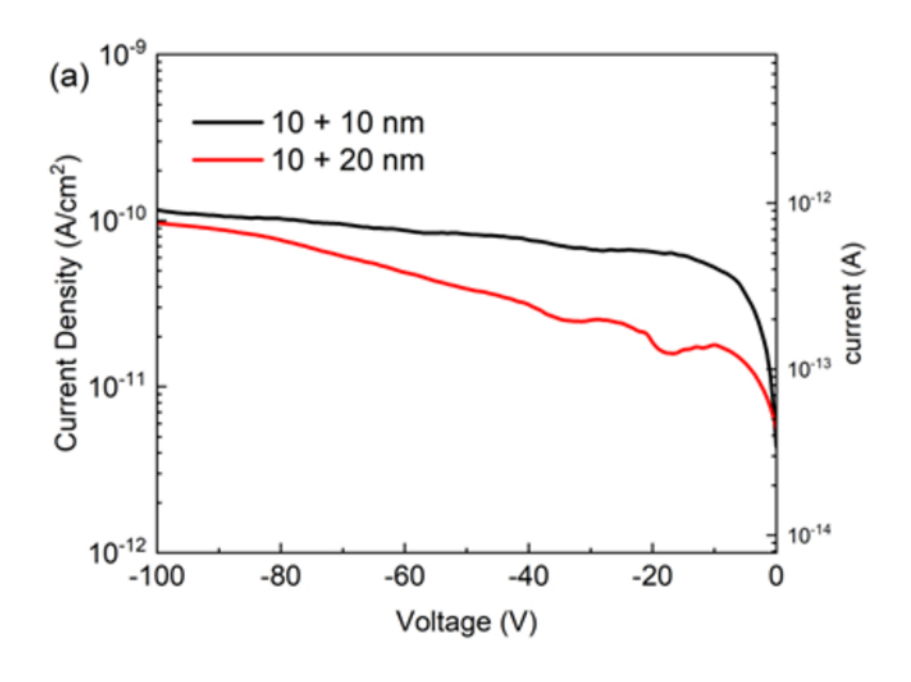
Journal of Vacuum Science

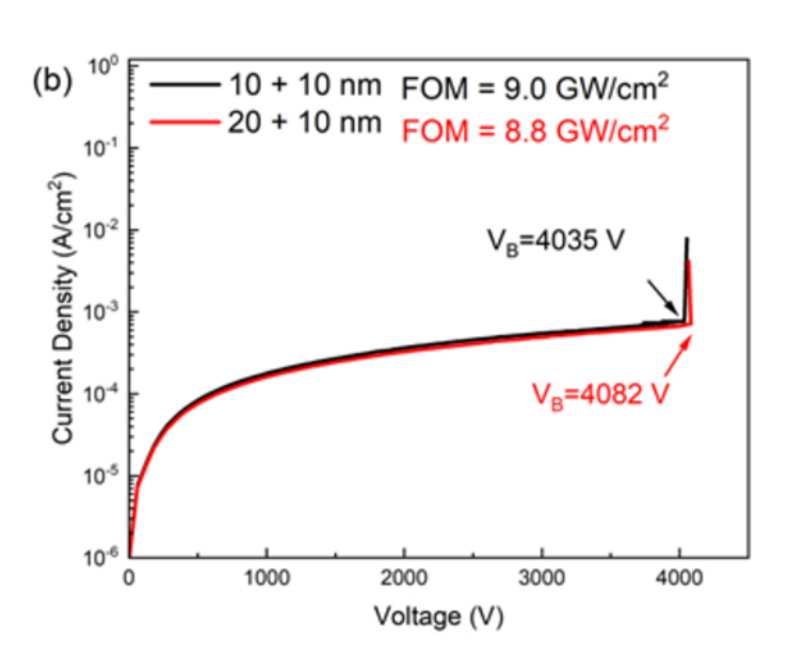




Technology A Vacuum Science Journal



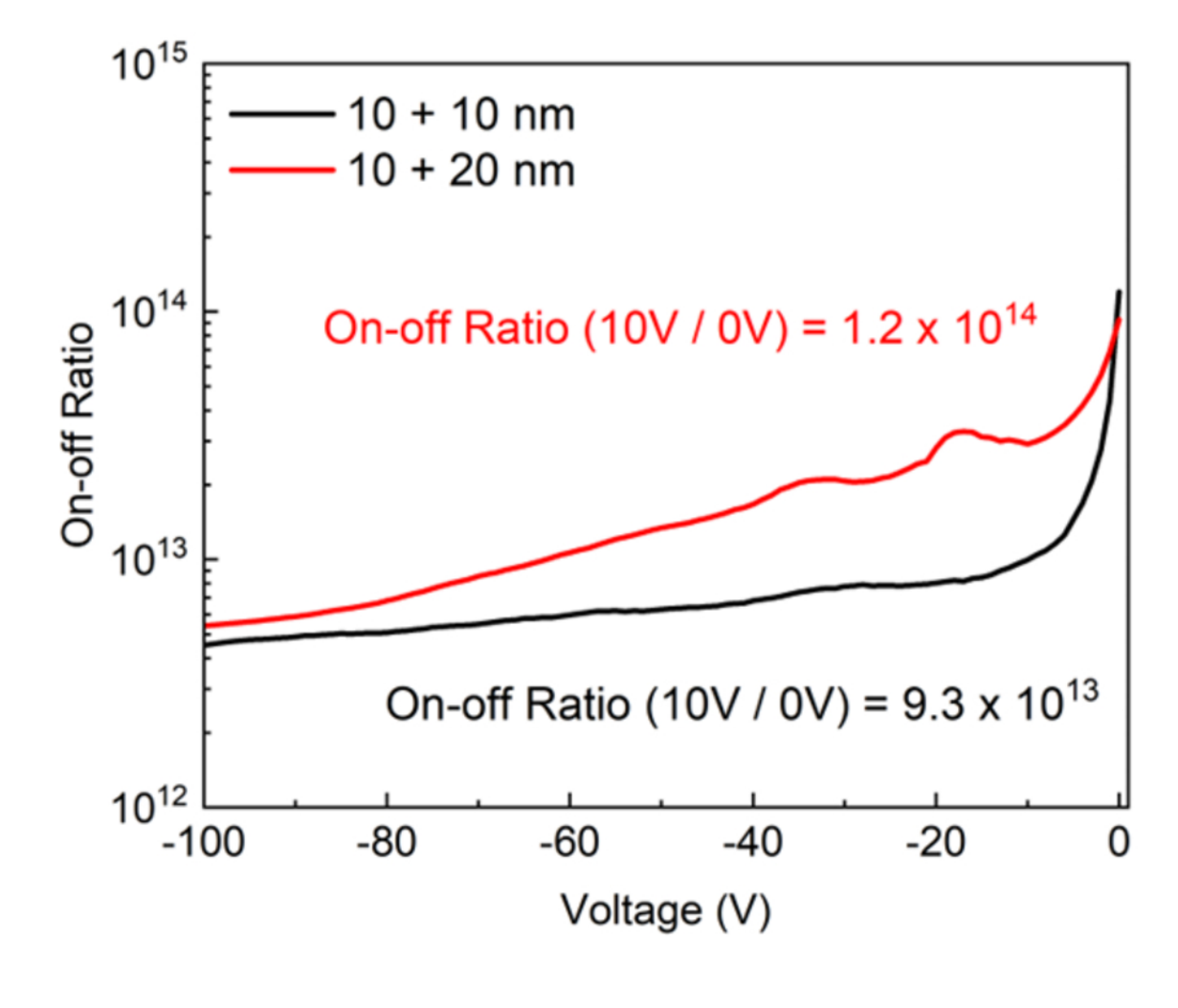






This is the author's peer reviewed, accepted manuscript. However, the online version of record will be different from this version once it has been copyedited and typeset.

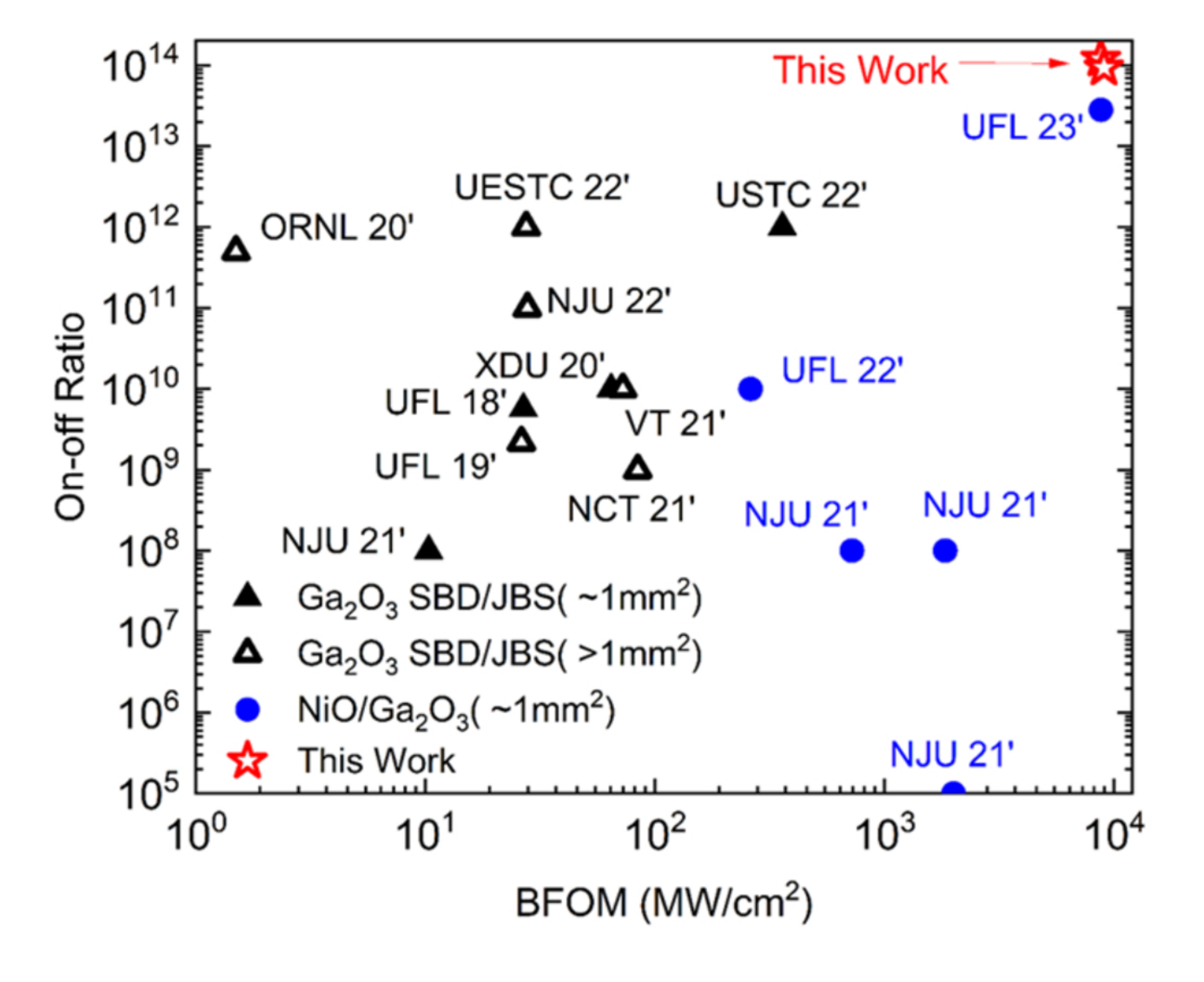
PLEASE CITE THIS ARTICLE AS DOI: 10.116/6.0002722





This is the author's peer reviewed, accepted manuscript. However, the online version of record will be different from this version once it has been copyedited and typeset.

PLEASE CITE THIS ARTICLE AS DOI: 10.1116/6.0002722



Journal of Vacuum Science & Technology



This is the author's peer reviewed, accepted manuscript. However, the online version of record will be different from this version once it has been copyedited and typeset.

PLEASE CITE THIS ARTICLE AS DOI: 10.1116/6.0002722

